Nano Today 25 (2019) 99–121

Contents lists available at ScienceDirect

Nano Today

journal homepage: www.elsevier.com/locate/nanotoday

Review

Nanostructured metallic transition metal carbides, nitrides, phosphides, and borides for energy storage and conversion

Khang Ngoc Dinh[a,b,1], Qinghua Liang[b,1], Cheng-Feng Du[b,c], Jin Zhao[b], Alfred Iing Yoong Tok[b], Hui Mao[d,*], Qingyu Yan[a,b,*]

[a] Energy Research Institute @ NTU (ERI@N), Interdisciplinary Graduate School, Nanyang Technological University, Singapore, 637553, Singapore
[b] School of Materials Science and Engineering, Nanyang Technological University, Singapore, 639798, Singapore
[c] State Key Laboratory of Solidification Processing, Center of Advanced Lubrication and Seal Materials, Northwestern Polytechnical University, Xi'an, Shaanxi, PR China
[d] College of Chemistry and Materials Science, Sichuan Normal University, Chengdu, 610068, PR China

ARTICLE INFO

Article history:
Received 28 November 2018
Received in revised form 17 January 2019
Accepted 26 February 2019
Available online 15 March 2019

Keywords:
Metallic transition metal-based nanomaterials
Enhanced electrical conductivity
Energy conversion
Energy storage
Electrochemical water splitting
Lithium ion battery

ABSTRACT

Metallic-like transition metal-based nanostructures (MLTMNs) has recently arisen as robust and highly efficient materials for energy storage and conversion. Owning to extraordinary advantages over the semiconducting/insulating ones (in terms of fast reaction kinetics, rapid electrical transport, and intrinsically high activity) combined with the high natural abundance, this class of materials is progressively developed towards commercial applications in real energy technologies. This review summarizes and discusses the progress in energy storages and conversions that employ MLTMNs. After the introduction and fundamental characteristics, developments in synthetic methodologies of MLTMNs and its application in energy storage and conversion are provided with more attention on strategies to improve electrochemical performances. Personal outlook on the challenges and opportunities of MLTMNs for industrial applications in real energy technologies are proposed and discussed in the conclusion.

Contents

* Corresponding author.
E-mail addresses: rejoice222@163.com (H. Mao), Alexyan@ntu.edu.sg (Q. Yan).
[1] These authors contributed equally to this work

https://doi.org/10.1016/j.nantod.2019.02.008
1748-0132/

Introduction

With the observation about the depletion of easily accessible fossil fuels and climate changes, the exploration of renewable form of energy conversions and energy carriers have turned out to be an important research topic. Regarding energy storage devices, secondary lithium/sodium-ion batteries (LIBs/ SIBs) and supercapacitors are considered as the key enabling devices [1]. Up to now, they have partly met our demands for compact but powerful energy storage. However, extending their application towards electric vehicles, military & aerospace applications, etc. requires much higher performance by means of rate capability, safety, energy density, and cyclability. To achieve those goals, the development of new electrode materials plays a crucial role. As for energy conversion technologies, transforming renewable energy (*eg.* wind, solar, etc.) to easily stored chemical energy (i.e. H_2) by electrocatalytic water splitting is of great potential, in which electrocatalysts for hydrogen evolution reaction (HER) and oxygen evolution reaction (OER) play a key role [2–5]. Then, to utilizing H_2 as a clean fuel in fuel cells, oxygen reduction reaction (ORR) also need to be facilitated to improve the efficiency. However, the current state-of-the-art electrocatalysts for these conversion processes are still based on precious metals (i.e. Pt [6] for HER, ORR and RuO_2/IrO_2 [7] for OER), which brutally hindered large scale applications. Hence, inexpensive and natural abundant alternatives with good catalytic performance and sturdiness over time are highly desired.

The combination of transition metals and elemental phosphorus, carbon, nitrogen, and boron give families of compounds; namely, phosphides, carbides, nitrides, and borides. Those materials, which exhibit significant advantages of being cheap, accessibility to synthesis at large scales and interesting properties, acquire a huge potential toward electrocatalysis and energy storage applications. On the other hand, it is well-known that different compositions (transition metal-rich or transition metal-deficient) can give rise to the changes in crystal and electronic structures, leading to metallic phase or semiconducting/insulating phases. Compared to transition metal -based phosphides/carbides/nitrides/borides that are semiconductors or insulators, the metallic ones with electronic structures similar to metals would have better conductivity facilitating electron transfer among layers, which is advantageous in electrocatalytic applications [8]; some of those metallic compounds are shown to have comparable performances to these of noble metals. In addition, the high electrical conductivity lowers the loss of electrical transport, enabling the significant improvement in performance of LIBs/SIBs or supercapacitors. More importantly, apart from good conductivity, those metallic transition metals compounds are more thermodynamically stable than the semiconducting/insulating ones and show favorable resistance to oxidation at high temperature (metallic-like properties of those materials are summarized in Table 1) [9,10]. Although these metallic transition metal phosphides/carbides/nitrides/borides have been tried out for various reactions (i.e. hydrogenation, hydrodesulfurization, amination, ammonia synthesis/ decomposition, hydrogenolysis, dehydrogenation, hydrazine decomposition, methanation, aromatization, isomerization, reforming, hydroprocessing, and water-gas shift) [9], there is still lots of interest and room for developments in their potential applications of improving existing battery technologies and energy conversion process (Fig. 1). Although there are some metallic transition metal chalcogenides having similar properties, they are mostly metastable and easily be transformed to semiconducting/insulating phases [11]; hence, will not be discussed in this summary.

Table 1
Metallic-like properties of carbides, nitrides and metal-rich phosphides[a]. Reproduced with permission from [9] Copyright 2008, Wiley-VCH.

	Phosphides and Carbides	Nitrides
Electrical resistivity ($\mu\Omega$ cm)	10 – 80	900 – 25000
Hall coefficient (10^{11} m^3 $°C^{-1}$)	−200 to 30	Unavailable
Magnetic susceptibility (10^6 emu mol^{-1})	6 – 30	110 – 260
Heat capacity (J mol^{-1} K^{-1})	30 – 80	20 – 50

[a] Principally, Group 4–8, first row.

In this review, we mainly summarize and discuss the progress in energy storages (LIBs/SIBs and supercapacitors) and conversions (HER, OER, ORR) that employ metallic like transition metal-based nanostructures (MLTMNs). Fundamental characteristics in terms of crystal structures are introduced. Then, we present comprehensive insight and recent advances of synthesis methods, energy storage and conversion applications with attention focused on strategies to promote performances of each type of metallic transition metal nanostructured. Lastly, we suggest our personal outlook on this promising class of materials to pave the way for future studies.

Phosphides

Phosphorus (P) forms transition metal phosphides (TMPs) with most of transition metals in the periodic table. However, as most of the P-rich TMPs are semiconductors or insulators and much less stable due to the fact that their electrons are localized in the neighborhood of P atoms [9,12], which will not be ideal for energy storage and conversion applications, the focal point of this section is on the transition metal-rich phosphides (MP, M_2P or M_3P, etc.), also called metallic transition metal phosphides (MTMPs) due to their metallic character.

The nature of MTMPs (and nitrides and carbides as will be discussed later) is a combination of physical properties of ceramics and electronic properties of metals; they are good heat and electrical conductors, hard and strong, and have high thermal and chemical stability [9]. Regarding the crystal structure, huge differences are observed between phosphides and carbides/nitrides. Interstitial structure, which is observed later on in many carbides and nitrides, is not feasible owning to the ~1.5 times bigger in size of P compared to N and C (0.109 nm of P to 0.071 nm and 0.065 nm of C and N, respectively). Instead, P is normally positioned in the center of the triangular prism made of metal atoms in MTMPs [13].

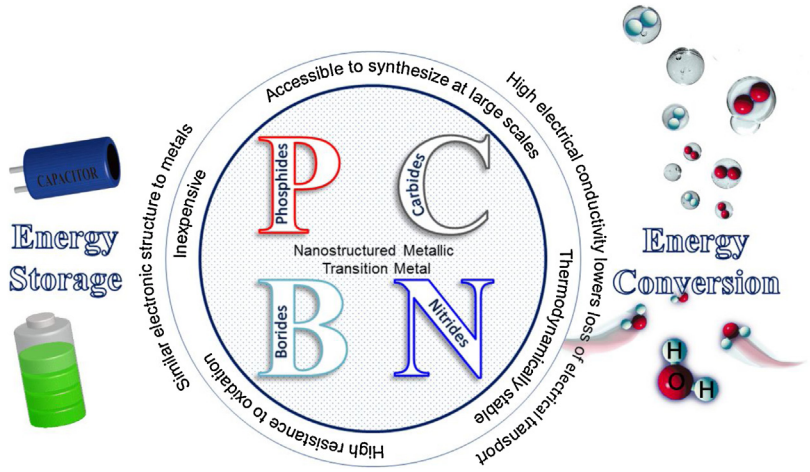

Fig. 1. An illustration \of the key properties and application of MLTMNs for energy storage and conversion.

There are a lot of publications related to MTMPs; however, in our perspective, most of them are very much alike in synthesis & characterization methodology, and performance analyses. In this part, typical synthesis methods of nanostructured MTMPs and their main application in energy storage/conversion are summarized and discussed accordingly; some typical and ground-breaking works will be analyzed in detail to give an in-depth understanding.

Synthetic methodologies of (MTMPs)

Generally, the synthesis of MTMPs can be classified by means of phosphorus sources. Regarding the application of energy storage and conversion, the source mainly comes from organic phosphines (i.e. trioctylphosphine, trioctylphosphine oxide, triphenylphosphine, alkyl- and aryl- phosphines) or inorganics (i.e. phosphate, elemental phosphorus, or hypophosphite). Importantly, the relative advantages and disadvantages of each type of P sources will be evaluated in detail.

Organic Phosphines (Oil-phase synthesis/ solution-phase) for MTMPs synthesis

The most popular organic phosphorus source in oil phase synthesis is trioctylphosphine (TOP). At the temperature of 300 °C and above, C–P bonds are broken and transition metal complexes (metal acetylacetonates, metal carbonyls) would be phosphidated under Ar or N_2 protective atmosphere. However, due to the above mentioned high decomposition temperature, the synthesis needs to be carried out with high boiling point organic solvents like 1-octadecene, octyl ether, oleylamine, and squalene which causes the reaction to be corrosive and flammable. The usage of those long chain organic solvents and TOP also leads to the difficulty in washing the products and normally requires an extra annealing step under O_2-free environment at elevated temperature (higher than boiling point of solvents/capping agents, usually ~400 °C) to remove those organic compounds. Attention should be also taken during this annealing step since a high temperature of above 500 °C would lead to serious sintering forming bulk phase instead of nanostructure.

Besides TOP, tri-octylphosphine oxide (TOPO) and other organic phosphines (*eg.* tri-phenylphosphine (TPP), alkyl- and aryl- phosphines) can be used in a similar manner or mixed with TOP [14–18]. This method was first considered as the general approach for synthesis of various TMPs including nickel phosphides [15,16,19,20], cobalt phosphides [14,17,21,22], iron phosphides [18], etc. Controlled compositions, morphologies, and sizes are obtainable through changing reaction parameters. In this regard, Brock et al. was one of the first to achieve the phase-pure hollow or solid $Ni_{12}P_5$ and Ni_2P nanoparticles with 10–32 nm in size just by tuning TOP: Ni ratio, temperature, reaction duration, and amount of solvent (Fig. 2) [23]. Specifically, at low TOP: Ni ratio metal-rich ($Ni_{12}P_5$) big hollow particles are formed, whereas small solid Ni_2P particles are formed otherwise. Higher reaction temperature and longer reaction duration is also found to favor the formation of more thermodynamically stable product – Ni_2P. Interestingly, metal-rich $Ni_{12}P_5$ was formed by increasing the volume of solvent (oleylamine in this case) regardless of TOP: Ni ratio; and volume of solvent could also be used to tune the void sizes of hollow $Ni_{12}P_5$ at a low TOP concentration. The formation of hollow structures (favored by low TOP concentration as mentioned) of Ni_2P is also possible by adding more TOP at crystallization temperature (~300 °C). Similar studies other than nickel phosphides were also conducted to further prove the versatility of the TOP route, i.e. Co_xP [22] and Fe_xP [24].

Remarkably, Brock and his colleagues reported the synthesis of MnP nanocrystals by organic phosphine route at record-breaking low temperature of 220 °C (note that C–P bonds are broken only at 300 °C and above) [25]. This was achieved with the help of tris(trimethylsilyl)phosphine which provides phosphorus source through redox neutral desilylation. However, most of the silylphosphines are extremely toxic (much more toxic than TOP) and ignite in air making it very difficult to handle; hindering their further uses.

Inorganic P and elemental P sources for MTMPs synthesis

As discussed above, the organic phosphines route has opened a shape, size, and composition controllable synthesis method for TMPs. Nevertheless, the sophisticated process is a big challenge for scale-up production. A better way is to employ inorganic phosphorus precursors. The most common method at the early days was via reduction of metal orthophosphate by H_2 or CH_4 only at high temperature (> 650 °C) due to strong P—O bonds. The mechanism was explained as after adsorbing to metal sites, H spills over to phosphate forcing the reduction [26]. Being mostly used for the synthesis of molybdenum phosphides and tungsten phosphides; however, this method is hardly ever used because of its energy-intensive; and more importantly, the products are usually in bulk form with large crystal size and irregular morphology, which limits the application for energy storage and conversions.

Classical source of phosphorus – elemental phosphorus is another source for phosphide nanoparticles synthesis. Unlike the phosphate reduction, the usage of milder conditions inhibits the aggregation of products. Surplus white phosphorus P_4, red phosphorus, and yellow phosphorus were used in hydrothermal and solvothermal reactions with molecular metal salts (chlorides,

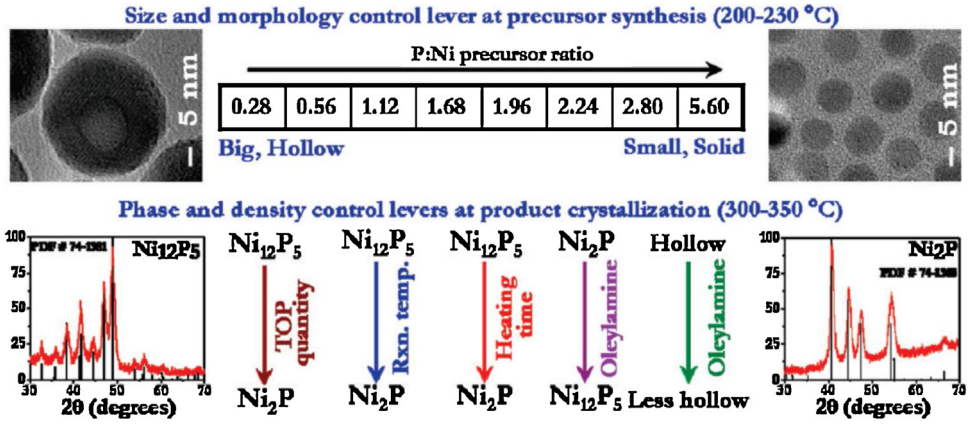

Fig. 2. Summary of the roles played by various synthetic levers in controlling the size, morphology, and phase in nickel phosphide nanoparticles. Reproduced with permission from [23] Copyright 2011, American Chemical Society.

nitrates, acetate, sulfate, etc.) at relatively low temperature (less than 200 °C) to prepare series of nanoparticles Ni_2P [27], $Ni_{12}P_5$ [28], nanocrystallites Ni_2P [29,30], Cu_3P [30], Co_2P [30,31], urchin-like Co_2P [32], and Fe_2P [33]. Complex structures can also be achieved by using mixtures of solvents, e.g ethylene glycol and water in case of nano-dendritical Ni_2P [34]. In addition, the cathodic electroreduction of Ni salts and dissolved P_4 in liquid ammonia at 160 °C gave Ni_2P nanocrystallites [35]. Our group was the first to successfully use black P (BP) as phosphorus source in solvothermal synthesis of phosphides [36]. An excess of exfoliated BP was reacted with nickel (II) chloride in DMF at 160 °C for only 3 h (fraction of 12-48 h when white/red/yellow P was employed). The reaction results in well-dispersed Ni_2P nanocrystals with an average diameter of 5̃ nm on BP heterostructure. Later on, there were a series of works that further proved the feasibility of this phosphide synthesis method, namely, in-plane black phosphorus/dicobalt phosphide (BP/Co_2P) heterostructures and hybrid Ni_2P/BP [37,38].

In addition to these inorganic phosphorus precursors described above, there is PH_3. The main problem is that PH_3 is extremely toxic and lethal even at a few ppm. Hence, hypophosphite that can generate PH_3 on-site, i.e. sodium hypophosphite (NaH_2PO_2) at around 250 °C are widely used as substitution: $2NaH_2PO_2 \rightarrow Na_2HPO_4 + PH_3$. The reaction is called pseudo-chemical vapor deposition (pseudo-CVD) in which the generated PH_3 upstream will be carried by protective gas flow (Ar or N_2) and react with various transition metal precursors (metal oxides, hydroxides, metal-organic frameworks (MOFs), and even metal some cases, etc.) in the downstream at 300–350 °C to produce TMPs. The biggest advantage of this method is to maintain the morphology of the downstream precursors. In addition, the reaction is facile, free of surfactant, wider ranges of transition metal precursors can be employed in comparison with organic phosphine routes, and the generated by-product Na_2HPO_4 in the upstream is easily washed away. While the above-listed method struggles when it comes to multi-metal phosphides (they normally form a mixture of transition metal phosphides), one of the few exceptions is presented by Taeghwan Hyeon and his colleagues in which NiFeP nanorods was synthesized by TOP route; however, even in this rare case, varied Ni: Fe ratios are difficult to achieve and maximum Ni content of 25% was obtained [39]. Nonetheless, this PH_3 route brings multi-metal phosphides synthesis to whole new level due to the versatility of metal precursors. For examples, start off with layer double hydroxides/MOF, NiCoP [40,41], $(Fe_xNi_{1-x})_2P$ [42], with tunable metal compositions and most recently $(V_xNi_{1-x})_2P$ by our group had been successfully synthesized [40–46]. Still based on phosphidation of metal precursor by on-site generated PH_3, a slightly modified method was presented by Liang et al. in which the hydrothermally synthesized NiCo-LDH/Ni foam was placed into plasma-enhanced chemical vapor deposition (PECVD) system, followed by PH_3 plasma treatment at 250 ° for 15 min [40]. Compared to the common PH_3 route described above, this small modification allows a lower temperature phosphidation at a much shorter time (15 min compared to ~1–3 hours).

Applications of MTMPs for Energy storage and conversion with strategies for enhancing performances

Electrode materials (Batteries and Supercapacitors)

Among the various electrode materials for Li and Na batteries, MTMPs have received lots of attention [47–49]. They have shown attractive Li and Na storage properties (theoretical capacity can reach 1̃200 mA h g^{-1} for LIBs and 9̃00 mA h g^{-1} for SIBs) through the conversion reaction: M_xP + 3Li (or Na) → Li_3P (or Na_3P) + xM [50]. Nevertheless, the practical application of these MTMPs is hindered by a serious capacity fading during cycling most likely due to irreversible conversion reaction and volume expansion.

To address that problem, Yu's group has developed the yolk–shell Sn_4P_3@C nanospheres as the advance anode for SIBs which restrains the problem of volume changes during cycling. The Sn_4P_3@C is composed of Sn_4P_3 nanoparticles shielded by a thin carbon layer. This yolk-shell structure with the void space suppressed volume expansion to a great extent. Besides, the self-supporting carbon shell can protect the Sn_4P_3 nanoparticles from surface oxidation. Hence, a specific capacity of 360 mA h g^{-1} at 1.5 A g^{-1} after 400 cycles [51]. Remarkable reversible specific capacity of 790 mA h g^{-1} at 100 mA g^{-1}, good rate capability (421 mA h g^{-1} at 3 A g^{-1}) were obtained as well. This strategy of suppressing volume expansion via porous/hollow structure and carbon confinement were then widely studied. CoP hollow nanoparticles encapsulated in amorphous carbon layer [22], Fe_2P nanoparticles enveloped in sandwich-like graphited carbon envelope nanocomposite (Fe_2P/GCS) [52], 3D porous molybdenum phosphide @carbon hybrid (3D porous MoP@C hybrid) [53], peapod-like C@NiCoP [54], and peapod-like composite with $Ni_{12}P_5$ nanoparticles encapsulated in carbon fibers [55] were reported as promising anode materials for LIBs and SIBs.

The utilization of MTMPs toward LIBs was also expanded through hybridizing with other materials like black phosphorus (BP) with which Ni_2P@BP is an example [36]. Due to its metallic nature, Ni_2P has tuned the charge carrier concentration; and consequently, increased electrical conductivity (from 2.12×10^2 S m^{-1} to 6.25×10^4 S m^{-1}). Moreover, the agglomeration of MTMPs nanoparticles could be prevented while they are dispersed all over the BP nanosheet; thus, higher surface area and larger number of active

sites for electrochemical reaction were obtained. As a result, much better Li ion storage properties compared to bare BP has obtained with ~4-fold higher in reversible capacity (1196.3 mA h g^{-1} at 0.1 A g^{-1}); high rate capabilities (322.0 mA h g^{-1} at 10 A g^{-1}), and decent long-term cycling performance of 94.1% capacity retention after 1000 cycles at 1 A g^{-1}.

Another type of energy storage device has gained lots of attention is supercapacitors. With good conductivity, MTMPs are also considered to be suitable as electrode materials for supercapacitors [56–58]. However, phosphides for supercapacitors application mostly relied on nickel phosphides or their composites, wherein the charge storage in alkaline condition is attributed to the Faradaic Ni^{2+}/Ni^{3+} redox couple.

$$Ni^{2+} + 2OH^- \leftrightarrow Ni(OH)_2$$

$$Ni(OH)_2 + OH^- \leftrightarrow NiOOH + H_2O + e^-$$

For examples, Ni_2P nanoparticles on reduced graphene oxide [59], amorphous Ni-coated Ni_2P [60], and Ni_2P grown on Ni foam [61] showed incredibly high specific capacitance (some even higher than RuO_2), and stable cycling performance. Apart from Ni_2P, Co_2P has recently been tried for supercapacitors [17]. Co_2P nanoflowers with the capacitance of 416 F g^{-1} at 1.0 A g^{-1} was revealed to be better than that of Co_2P nanorods (284 F g^{-1}). Good cycling stability was observed as well with 97% specific capacitance retention after 600 cycles. When employed as an anode in asymmetric supercapacitor (graphene as cathode), high energy and power densities were obtained (8.8 Wh kg^{-1} at 6 kW kg^{-1}). These results pave new ways to expand the scope of MTMPs for supercapacitor other than Ni_2P; even though, finding new MTMPs with high capacitance and large potential window are of big challenge.

Electrocatalysts (HER, OER, and ORR)

More than a decade ago, theoretical calculation has already predicted that Ni_2P (001) is a promising candidate to replace Pt for HER [62]. However, it was not until 2013 when Popczun et al. [19] reported high HER performance of Ni_2P hollow nanoparticles and paved the way to MTMPs research toward electrocatalysis. The prepared Ni_2P showed high density of exposed (001) facets; hence, an expectedly high exchange current density of 3.3×10^{-5} mA cm^{-2} and a low Tafel slope of ~46 mV dec^{-1} were obtained. Since then, nickel phosphide family ($Ni_{12}P_5$, Ni_5P_4) [15,16,20], cobalt phosphide family (CoP, Co_2P) [21,63], MoP [6,64,65], WP [66], FeP [18], and Cu_3P [67] were also reported as very active and durable electrocatalysts for HER.

With good HER performance, MTMPs were also expected to have good OER electrocatalytic activity due to several reasons. First, bifunctional OER and HER catalysts would streamline water splitting devices and make it much more possible at industrial scales. Secondly, the surface of MTMPs can be easily oxidized during high oxidative OER condition to give hydroxides/oxyhydroxides surface which was proven to be highly active toward OER. However, only metallic nickel and cobalt-based phosphides were studied intensively; most likely due to the good OER activity of Ni or Co-based hydroxides/oxyhydroxides [68–70].

Recent years witness lots of publications that directly grow MTMPs on 3D conductive substrate like Ti foil, carbon cloth, carbon paper, or Ni foam, etc. With this way, better mechanical adhesion between MTMPs and substrate is obtained without binders, resulting in promoted charge-transfer in comparison with conventional post-transferred to the substrate, which later on has a big impact on electrocatalytic HER and OER performance. For example, FeP [71], Ni_2P [72], and CoP [73] were grown on carbon cloth/carbon paper and showed significantly improved current density (by 5–6 times) at given overpotential compared to the normal ones. In addition, a direct growth on conductive substrate would make the electrode hydrophilic and aerophobic at the same time; hence, facilitating mass transfer and addressing the gas bubble adhesion problem during electrolysis. This phenomenon has been widely observed in the cases of Ni_2P and Cu_3P [67,74].

Hybridizing with carbon (carbon nanotubes, graphene, porous carbon) or phosphorus is another possible way to improve electrocatalytic activity through fully capitalize all the active sites by good dispersity. On top of that, the coupled C or P can modulate electron density and electronic potential distribution of the heterostructure [75]. Taking the synthesized BP/Co_2P by Wang and his co-workers as an example, BP/Co_2P showed much improved HER and OER performances in alkaline condition (pH = 14) [38]. Similar results were also seen in the case of Ni_2P@BP [36] which needs only -107 mV at -10 mA cm^{-2}; while the values for Ni_2P and bare BP are at -311 and −600 mV. The electrode indicated fast kinetics as well, shown by Pt-like Tafel slope of 38.6 mV dec^{-1}. Another example is carbon nanotubes decorated with CoP nanocrystals (CoP/CNT) that showed much enhanced HER performance than bare CoP (-122 mV of CoP/CNT compared to -226 mV of CoP to drive -10 mA cm^{-2}) [76].

Another strategy to improve their catalytic activity is to dope MTMPs with other transition metals. In this regard, the PH_3 route offers the best way to achieve multi-metal phosphides which normally shows better catalytic activity toward single metal ones, which has been proven theoretically and experimentally. Theoretically, guidance by DFT calculations, a much-increased density of state (DOS) intensity of NiCoP compared to Ni_2P indicates faster charge transfer kinetics. In addition, D-states of NiCoP is shown to be closer to Fermi level in comparison with Ni_2P, suggesting a lower OH^- adsorption energy which is normally the rate-determining step (RDS) of OER (Fig. 3a-b, d–e) [40,41]. Regarding HER, it can be traced back to a decade ago when TMPs were famous for hydrodesulfurization (HDS) catalysis, TMPs were expected to have good activity toward HER as well. Since what important in both HDS and HER are the adsorption/desorption reversibility of H on the catalyst surface. HER consists of 2 steps (initial state of $H^+ + e$, intermediate H* where* is the adsorption site, and ½H_2 as product) in which the Gibbs free energy for H adsorption (ΔG_{H^*}) is usually employed to predict the HER catalytic activity [40]. According to Sabatier principle, the H binding should be neutral ($\Delta G_{H^*} = 0$), either too strong or too weak binding would result in blockage of active sites or sluggish reaction, respectively. In this respect, the most stable surface of NiCoP, which is NiCoP (0001), revealed the ΔG_{H^*} value significantly close to 0 than that of Ni_2P (−0.15 and −0.14 eV compared to −0.86 eV and −0.45 eV for sites 1 and site 2, respectively) (Fig. 3c). Another point needs to be considered is that the HER reactions in neutral and basic environments require a prior step of water dissociation, and the adsorption energy of H_2O molecules on both Ni_2P (0001) and NiCoP (0001) mark the value of ~18 eV, even higher than Pt (111) at 8.97 eV suggesting NiCoP is a promising HER electrocatalyst to replace Pt in non-acidic condition (Fig. 3f). Experimentally, Kuang and co-workers developed $NiMoP_2$ nanowire that required only -195 mV to drive -100 mA cm^{-2} with a Tafel slope of 56 mV dec^{-1}, surpassing single metal TMPs Ni_5P_4 and MoP [44]. Another study that took advantage of this concept was presented by Seong Chan Jun's group [77]. Derived from NiCoFe-LDH, their $NiCoFe_xP$ indicated a decent overpotential of 39 mV at -10 mA cm^{-2} toward HER alongside with a Tafel slope of 50 mV dec^{-1}; while all other double metal phosphides show poorer performances, i.e. NiFeP (109 mV, 112 mV dec^{-1}); CoFeP (91 mV, 102 mV dec^{-1}); NiCoP (86 mV, 88 mV dec^{-1}). Considering the other half of water electrolysis – OER, similar performance trend was observed in which $NiCoFe_xP$ (η_{50} of 275 mV, and Tafel slope of 56 mV dec^{-1}) outperforms other double metal phosphides and even the benchmark RuO_2 by a great margin.

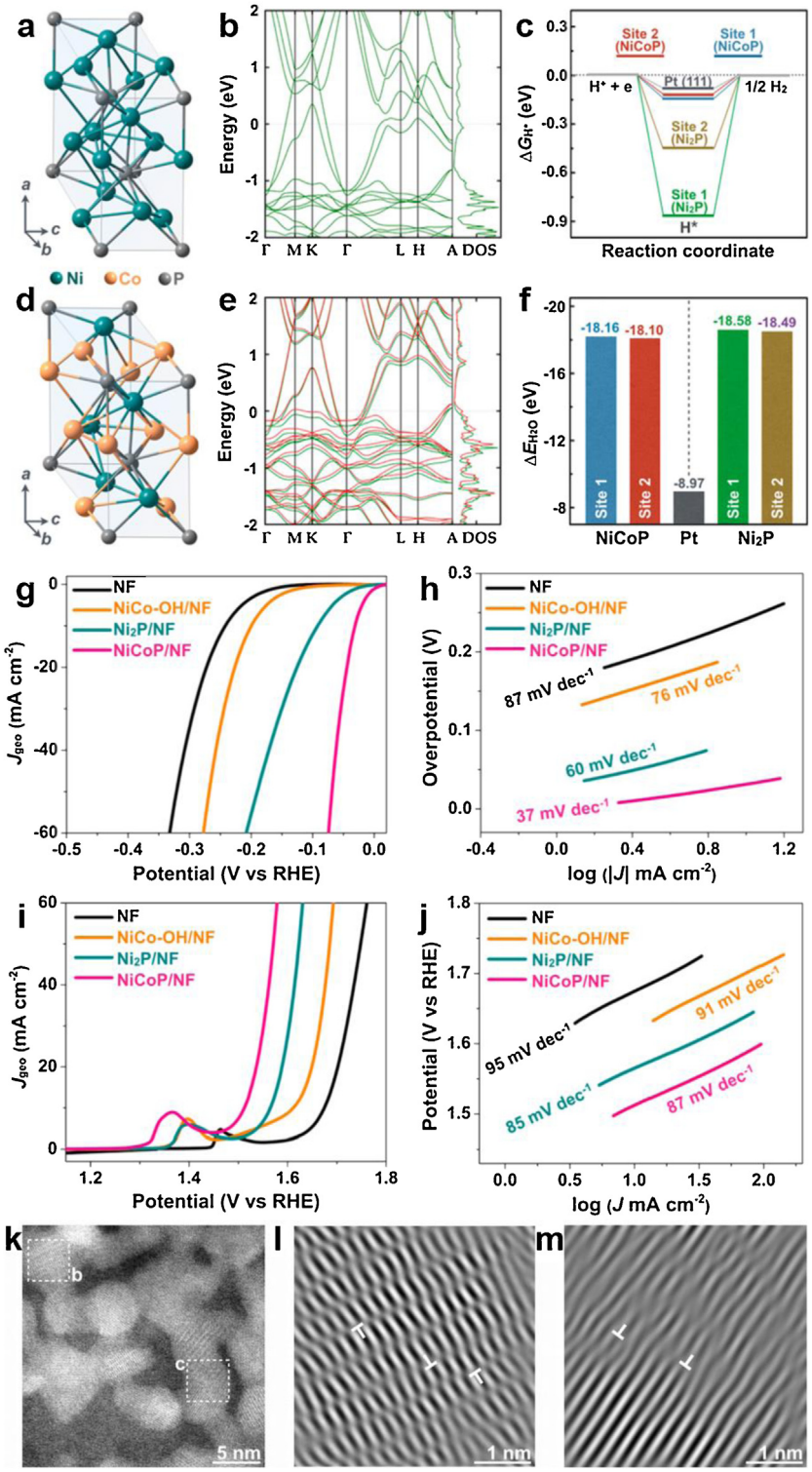

Fig. 3. (a,d) Crystal structures in unit cell of Ni_2P and NiCoP. (b,e) Electronic band structures and PDOS of the bulk Ni_2P and NiCoP (spin-up, green curves; spin-down, red curves). (c) Free-energy diagram for H adsorption. (f) Adsorption energy for H_2O. (g–h) HER and (i–j) OER electrocatalysis in 1.0 M KOH. (g,i) IR-corrected polarization curves and (h,j) their corresponding Tafel slopes. (e) STEM annular dark field (ADF) image of the NiCoP. (f,g) Inverse Fourier-filtered images of the squares marked areas in a showing the presence of edge dislocations. Reproduced with permission from [40] Copyright 2016, American Chemical Society.

Advances in synthesis methodology also attribute to the electrocatalytic performance of MTMPs [40]. The NiCoP synthesized by PH_3 plasma via PECVD system described above was evaluated toward HER and OER application (Fig. 3g-j). Not surprisingly, the NiCoP exhibited a substantially better activity than Ni_2P and NiCo-LDH. In addition, the utilization of PH_3 plasma not only offers the facile TMPs synthesis at lower temperature but also provides defect-rich nanosheets which can be observed through the uniform distributed nanopores in the TEM images and the presence of edge dislocations in the STEM inverse Fourier-filtered images (Fig. 3k-m). This defect-rich structure would grant higher electrochemically surface active area, increase electrolyte diffusion to

better utilize the active sites; consequently, boost up the electrocatalytic activity. Therefore, toward HER, the NiCoP by PECVD method showed a current density of -10 mA cm^{-2} at only 32 mV overpotential and Tafel slope of 37 mV dec^{-1}, which is much better than 86 mV and 88 mV dec^{-1} of the NiCoP synthesized via common PH_3 route presented by other works [77]. The OER performance shows similar pattern where overpotential at specific current density and Tafel slope of the former is notably lower than the latter (~330 mV and 87 mV dec^{-1} compared to 346 mV and 121 mV dec^{-1}). Very recently, our group reported a combined-strategy of cation tuning and surface engineering into Ni_2P nanosheets [78]. The resultant oxygen plasma treated V-doped Ni_2P shows noticeably improvement toward HER and OER, which were attributed to the better charge transfer kinetics and enhanced wettability.

Regarding ORR – an important counterpart to HER in Proton-exchange membrane fuel cell, MTMPs is normally added to carbon materials to improve the performance [79–81]. For example, Huang *et al.* prepared a series of MTMPs (Mn_2P, Co_2P, Ni_2P) nanoparticles and individually hybridized with doped carbon nanotubes (HCNT) forming core (nanoparticles)/shell (carbon) structure [79]. Among those MTMPs, HCNTs–Co_2P and HCNT–Mn_2P presented favorable kinetics with average electron transfer number of 3.52–3.78, much closer to the desirable 4-electron process as compared to that of HCNTs–Ni_2P (2.89–3.37). In addition, low overpotential, superior methanol tolerance, and high stability were obtained. This astonishing performance was explained by the host-guest electronic interaction (MTMP nanoparticles core and CNT shell). Concretely, the strong electron donating property of Mn_2P, Co_2P pushes the p electrons of the doped carbon to higher HOMO, making it more susceptible to oxidation; and hence, better catalytic activity. However, there was not much of experimental evidence to support the proposed electronic interaction. Therefore, more comprehensive efforts are needed to address the real catalytic active sites, catalytic mechanism, and improve the performance of MTMPs towards ORR.

Carbides

Due to the advantages of high electrical conductivity, excellent chemical stability, and intrinsic catalytic activity, transition-metal carbides (TMCs) have been widely studied as active materials for various applications, such as batteries, electrocatalysis, and fuel cell. Normally, all the transition metals from group IVB to VIB can be able to form TMCs except the Pt-group metals. Normally, the TMCs have the same crystal structures as their parent metals since the smaller carbon atoms tend to locate at the interstitial sites of the parent metals. Owing to the different intrinsic structures and physical properties of metals, the TMCs usually have three different kinds of formulas, namely, MC, M_2C, and M_3C. The monocarbides like TiC, ZrC, TaC usually crystallize in cubic texture as NaCl, while the M_2C and M_3C have much more complex atomic arrangements by forming orthorhombic and hexagonal structures. Accordingly, the physical & chemical properties of the TMCs are highly dependent on their crystal and electronic structures. Overall, the TMCs show the integrated properties of covalent solids, transition metal, and ionic crystals [82]. Typically, some metallic TMCs (MTMCs) not only show comparable electronic conductivity as parent metals but also have similar catalytic properties as precious Pt-group metals. As such, this category of MTMC materials has been attracting increasing attention in fundamental studies as well as practical applications in many fields. Typically, as a 2D family member of MTMC materials, metallic "MXene" materials, developed by Gogotsi's group in recent years, are emerging as highly fascinating materials, have been well documented and established in many recent reviews [83–85]. Considering the rapid development in this field, in this section we will mainly discuss recent advances of the MTMCs beyond MXene that are promising materials for energy storage and conversion applications with low-cost and environmental friendless, such as TiC, Ni_3C, Co_2C, MoC, and WC, *etc*.

Synthetic methodologies for MTMCs

As known, the design and preparation of high quality MTMCs are highly important to explore their applications in energy storage and conversion fields. To achieve a good performance, MTMC architectures with a high specific surface area and many accessible active sites are preferable. In the following sections, we will focus on reviewing some recent advances in the preparation of typical MTMC nanostructures, including carbothermal methods, controllable deposition approaches, wet strategies, and other alternative methods. The relative strengths and weaknesses of each synthetic methodologies will be discussed with regards to their applications.

Carbothermal methods are the most commonly used method for the preparation of MTMCs. The reaction mechanism for this method is the direct carbonization of metal or metal oxides. As such, this method usually involves the mixing the precursors of metal and solid carbon followed with a long-time thermal treatment at an extremely high temperature over 1200 °C. The traditional carbothermal methods often produce metal carbides in a large scale but with large particle size caused by the high temperature. In order to decrease the reaction temperature as well as control the morphology and size of the final products, the carbon and metal reactants are usually required to be specially designed. Biomass carbon like cotton and plants have been widely used as both carbon sources and growth templates due to the low-cost and unique architectures [86–88]. Besides, graphene has been also widely explored as the carbon source and substrate to prepare various nanostructured MTMCs with good tailored dimensions and morphologies [89–91]. For example, our group achieved the preparation of unique 3D interconnected TiC nanoparticle chains by using macroporous graphene/TiO_2 aerogels as the precursors [92]. The graphene not only serves as the carbon source but also as the growth substrate to regulate the size of the final TiC nanoparticles. Despite of the universality of carbothermal methods, the inhomogeneous carburization at high reaction temperatures make it still difficult to prepare MTMCs with well-controlled structures due to the serious aggregation.

The controllable deposition approaches like CVD/PVD are usually used to produce thin MTMC films or crystals with clean surfaces. The reaction mechanism of this method is direct carbonization of metal surfaces under carbon atmosphere. The deposition approaches often refer to the usage of hydrocarbons (e.g. CH_4, C_2H_6, or their mixtures, *etc*.) as the carbon sources. This is good for decreasing the carbonization temperature as well as growing high-quality crystals with exposure of specific facets. For example, Xu et al., achieved the growth of large-area high-quality 2D ultrathin α-Mo_2C crystals over 100 μm in size on Mo foil by CVD method [93]. They found that a low concentration of methane and the fast cooling after CVD growth are vital for the preparation of ultrathin α-Mo_2C crystals with clean surfaces. Such 2D α-Mo_2C crystals were found to be mainly exposed with (100) facets, as shown in Fig. 4. Similarly, this method could be also used for preparing 2D high quality ultrathin WC and TaC crystals along [0001] and [111] facets. Besides, the deposition method can be used to produce MTMCs with heterostructures. Recently, Zeng and co-workers developed a liquid-metal-solvent based co-segregation (LMSCS) strategy to direct fabricate 2D WC/graphene nanojunctions over a large-scale [94]. Although the deposition approaches have many advantages, the high cost of hydrocarbon reactants and complicated post-treatments hinder their large-scale productions.

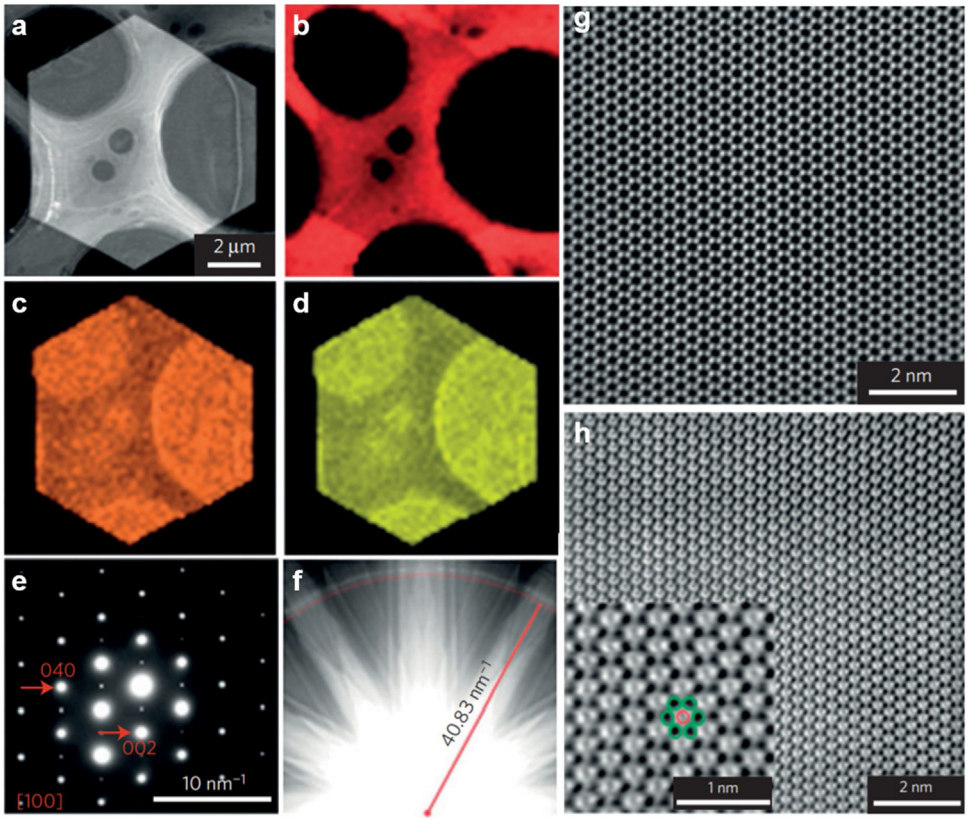

Fig. 4. Characterization of 2D ultrathin α-Mo_2C crystals. (a) Low-magnification ADF-STEM image of a hexagonal 2D α-Mo_2C crystal. (b–d) EDS elemental mapping of (b) C–K, (c) Mo-K, and (d) Mo-L lines. (e) SAED pattern along the [100] zone axis. (f) CBED pattern along the [100] zone axis. (g) Atomic-level HAADF-STEM and (h) BF-STEM images of the α-Mo_2C sheet in a (Mo atoms: white dots in g, C atoms: black dots indicated by red circle in the inset of h). Reproduced with permission from [93] Copyright 2015, Nature Publishing Group.

Wet chemical approaches are highly advantageous over the traditional high-temperature methods for preparing MTMC nanomaterials. On one hand, this method can be carried out at much lower temperatures (less than 400 °C). This is favorable for lowering the cost and reduce energy consumption. Furthermore, this method is able to control the morphology and phase of the final MTMC products. At this relatively high reacting temperature, liquid polyol solvents are usually explored as the medium due to their high boiling points. Besides, inert gas protection and the use of appropriate surfactants or other capping agents are often employed to prevent the oxidation of metal ions as well as control the growth rate of particles. For example, Harris and co-workers realized the preparation of acicular cobalt carbide nanostructures composed of Co_3C and Co_2C phases by using a single-step polyol reduction of metallic cobalt salts at ~300 °C [95]. Poly-vinylpyrrolidone (PVP) and NaOH were used to adjust the ratio of phase composition, volume, particle sizes, as well as the packing density. Chen et al., reported the preparation of urchin-like Co_2C/Co_3C nanoparticles in size from 180 to 290 nm by refluxing Co^{2+} in polyethylene glycol-200 medium at 270 °C for 3 h under a N_2 atmosphere [96]. Metallic Co_2C nanoflakes with exposure of (020) facet could be prepared by reduction of Co^{2+} in the mixed solvent of triethylene glycol and oleylamine at 300 °C for 3 h under Ar atmosphere [68,97]. These studies well-demonstrated the controllable growth of MTMC nanomaterials at a low temperature. The disadvantageous of wet strategies, such as relatively small-scale preparation, time consumption for post-washing processes, and high cost of polyol and gas protection, may limit their commercial applications to some extent.

In recent years, some other alternative methods have been developed for MTMC nanostructures, like mechanical ball milling [98], direction carbonization of novel precursors [99–101], and so on. Typically, preparing MTMC nanomaterials by a direct carbonization of metal-organic frameworks (MOFs) under inert gas atmosphere is emerging as an effective strategy [100,102]. Due to the presence of both organic ligands and metal cations, no additional carbon and metal sources are needed. Besides, the uniform distribution and protection of organic ligands make it is easy to obtain ultrasmall MTMC nanocrystals distributed homogeneously on carbonaceous matrix with uniform size due to the confinement of organic ligands. Such MTMC/C hybrid is favorable for electrocatalytic and energy storage and conversion applications [102]. For example, our group recently prepared ultrafine Fe-doped Ni_3C nanodots (~3 nm) dispersed well in N-doped carbon nanosheets by annealing 2D nickel cyanide coordination polymer precursors under Ar atmospheres at 400 °C. [99] 3D porous molybdenum carbide with hierarchical structure and high specific surface area were also obtained by using the porous nitrogen-doped carbon framework as both template and carbon precursor [103]. Wu and his colleagues reported the preparation of mesoporous MoC_x nano-octahedrons composed of ultrafine nanocrystallites by a carburization of metal-organic frameworks composed of copper and molybdenum at 800 °C under N_2 flow [102]. Besides, there are some other newly developed strategies for the atomic-scale controlled preparation of MTMCs. Recently, Sang et al., proposed a bottom-up synthesis method for the synthesis of TiC single layer on surfaces of MXene substrates by thermal exposure activation and electron-beam irradiation [104]. Although this strategy is unable to prepare MTMC on a large scale, it is practicable for the growth of higher quality single-layer MTMCs for insightful fundamental studies.

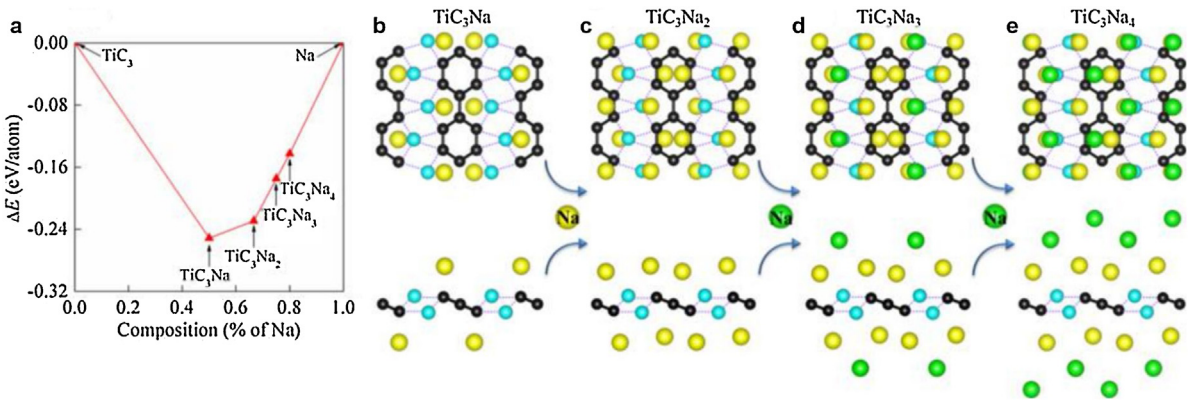

Fig. 5. (a) Relative stabilities of TiC_3Na_n (n = 1–4) with respect to an elemental solid Na and TiC_3 monolayer at 0 K. The optimized monolayers corresponding to the data points located on the convex hull are thermodynamically stable. (b–e) The most stable structures with different Na concentrations in TiC_3Na_n (the Na atoms of the first and second adsorbed layer are marked by yellow and green, respectively). Reproduced with permission from [118] Copyright 2018, American Chemical Society.

Applications of MTMCs for Energy storage and conversion with strategies for enhancing performances

The high intrinsic conductivity and catalytic activity, and good chemical stability make MTMCs to be good candidates for promising electrocatalysts and electrode materials for energy storage and conversion. There are several good reviews about the use of metal carbides for electrochemical energy storage in recent years [85,105–109]. In this section, we will focus on summarizing some new progress about using MTMCs for energy storage (supercapacitors, LIBs/SIBs) and electrocatalysis (OER, HER, and ORR) and show some mechanistic discussions for comprehensive understanding.

Electrode materials (Supercapacitors and batteries)

The good intrinsic conductivity enables the MTMCs to be highly attractive electrode materials for various batteries such as lithium ion [110–115], sodium ion [116–119], and supercapacitors [120]. Yu et al., explored first-principles to search the potential use of 2D Ta_xC_y as the anode for LIBs [121]. They found that the increase of the carbon composition in the Ta_xC_y would help to increase specific capacity and decrease the diffusion energy barrier. As such, designing C-rich 2D MTMCs is possibly a good strategy to improve performance towards LIBs. Apart from the composition, the structures include the size and morphology can greatly affect the electrochemical performance of MTMCs for LIBs. For example, our group designed a 3D interconnected TiC nanoparticle chain that could deliver 450 mA h g^{-1} and 137 mA h g^{-1} at 0.1 A g^{-1} and 20 A g^{-1}, respectively [92]. More importantly, a stable capacity of 170 mA h g^{-1} could be still obtained after 8000 cycles at 10 A g^{-1}. Such remarkable Li-storage properties are attributed to the fast ion and electron transport contributed from the high intrinsic conductivity and 3D interconnected porous structure. A similar 3D porous Mo_xC@N-C with Mo vacancies was reported to show a high discharge capacity of 825.3 mA h g^{-1} at 0.5 A g^{-1} [122]. The 3D porous structure combined with Mo vacancies resulted in more active sites, easier penetration of the electrolyte, and faster diffusion of ions. As such, a capacity of 266.6 mA h g^{-1} could be achieved despite a high current density of 5.0 A g^{-1}.

In addition to LIBs, MTMCs also of great potential for SIBs. For example, Yu and coworkers theoretically predicted that metallic TiC_3 monolayer with C_2/m symmetry is an attractive anode for SIBs with a high capacity of 1278 mA h g^{-1} as well as an extremely low barrier energy (0.18 eV) and open-circuit voltage (0.18-0.5 V) (Fig. 5) [118]. They found that the TiC_3 monolayer maintains metallic properties even after absorbing sodium atom due to the containing of zig-zag Ti atom chain and n-biphenyl unit. They further demonstrated that such TiC_3 monolayer functionalized with oxygen was able to improve the Na-ion storage capacity. Also, the presence of covalent, ionic, and metal bonds enables the feasible preparation in practical experiments. These results are instructive for the development of promising MTMCs for SIBs. Furthermore, to afford a stable Na-ion storage performance, the MTMCs are usually hybridized with carbon nanomaterials to prevent rupturing during cycling process. For example, Li et al., reported the in situ formation of ultrafine MoC nanoparticles inside the pores of graphitic carbon matrix as anode for SIBs [119]. The abundant pores of the highly conductive carbon support and the ultrafine structure of MoC nanoparticle was able to alleviate stress, accommodate large volume changes, and improve the transport of electrons and electrolyte during the repeated charging-discharging processes. A stable discharge capacity of 250 mA h g^{-1} could be delivered after 50 cycles at 0.05 A g^{-1}.

Besides that, there are also few studies reported MTMC nanostructures as the electrode materials for supercapacitors [120,123,124]. This is mainly ascribed to the outstanding electrical conductivity and excellent chemical stability. In order to achieve a high capacity for supercapacitor, MTMCs were usually designed with high specific surface area. For example, Fan and co-workers prepared 3D tubular all-TiC hierarchical fibres (HFNT TiC) by carbothermal method using the commercial T-shirt cotton fibers as both template and carbon sources [120]. Such HFNT TiC was highly porous and showed a high specific surface area of 255 m^2 g^{-1}. An extremely high capacitance of 185 F g^{-1} at 2.0 A g^{-1} and a remarkable cycling stability at high-rates even at low temperature (67% retention at −15 °C after 50,000 cycles) were realized in such HFNT TiC when used as electrodes for supercapacitors. Overall, these studies highlight the advantages of nanostructured MTMCs with high intrinsic conductivity and more active sizes for promising energy storage applications.

Electrocatalysts (HER, OER, and ORR)

The MTMCs like MoC_x and WC_x have been widely employed as efficient electrocatalysts due to high resistance to CO poisoning, superior corrosion tolerance over the whole range of pH and potential; and more importantly, their highly similar electronic structures as platinum [125]. It can be traced back to as early as 1974, detailed valance band examination by X-ray photoelectron spectrum demonstrated that the electronic states of tungsten carbide (both WC and W_2C) were more similar as that of platinum than the corresponding tungsten metal [125,126]. With the great promise to replace the commercial precious metal-based electrocatalysts, various MTMCs have been widely studied as the electrocatalysts for HER [90,94,127–130], OER [87,99,131–134], and ORR [91,135–137]. In order to enhance the catalytic per-

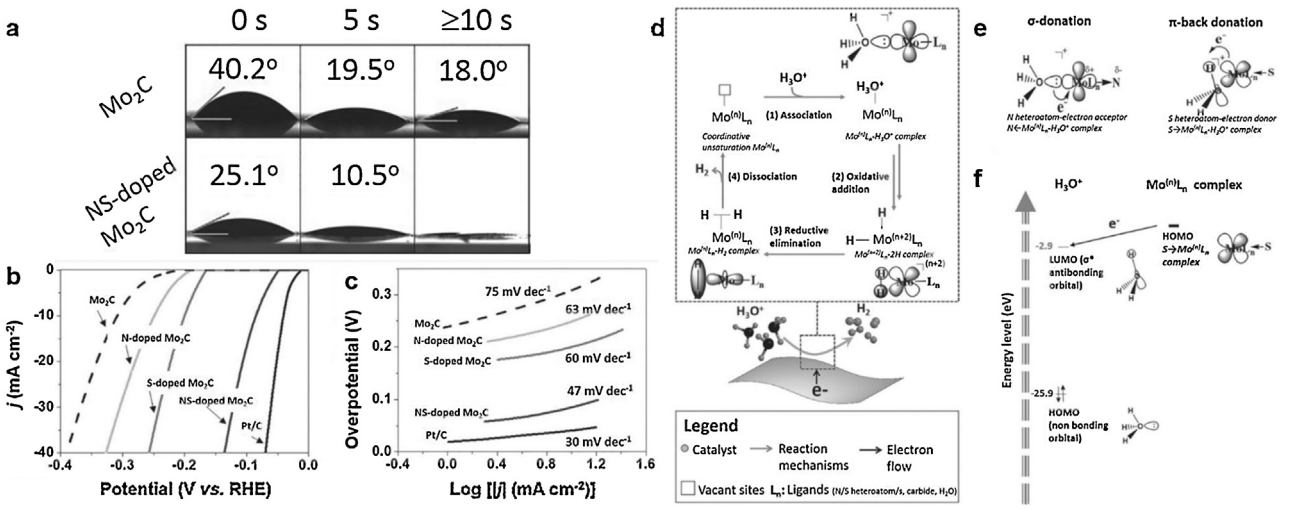

Fig. 6. (a) Contact angle measurement for the pure Mo_2C and NS-doped Mo_2C nanosheets. (b) Polarization curves of Mo_2C, S-doped Mo_2C, N-doped Mo_2C, NS-doped Mo_2C and Pt/C in 0.5 M H_2SO_4 and (c) their corresponding the Tafel plots. (d) Schematic of proposed catalytic cycle for HER. b) Proposed mechanism for adjacent N–S (electron-acceptor and electron-donor) pair doped in Mo_2C. c) The energy diagram of the H_3O^+ molecular orbitalsand $S\rightarrow Mo^{(n)}L_n$ complex with its highest occupied molecular orbital (HOMO). Reproduced with permission from [101] Copyright 2015, Wiley-VCH.

formance to realize their potential, there are increasing number of reports on developing MTMCs by various strategies, such as decreasing size, design proper architectures, incorporation of conductive substrates, and defects engineering. Most of these attempts aim to improve the reaction kinetics by increasing the active sites as well as exposing more active sites to the electrolytes. For example, Zhang and co-workers report the ultrasmall MoC_x (~2.8 nm) and WC_x (~2.0 nm) nanoparticles encapsulated in porous N,S-codoped graphene matrix with excellent HER activity in a broad range of pH, showing potentials of −130 mV, -150 mV, and −140 mV at -10 mA cm^{-2} in pH = 0, 7.2, and 14, respectively [130]. Such excellent HER performance is attributed to the abundant catalytically active sites as well as the good electrical conductivity. Recently, our group designed novel 2 *at%* Fe-doped Ni_3C nanodots encapsulated in N-doped carbon matrix demonstrates low overpotentials and modest Tafel slopes in 1.0 M KOH for both HER (292 mV, 41.3 mV dec^{-1}) and OER (275 mV, 62 mV dec^{-1}) [138]. The nanoporous N-doped carbon matrix not only could prevent the aggregation of Ni_3C nanodots but also increase the electronic conductivity as well as the number of active sites for fast electrochemical dynamic. Besides the physical and structural optimization methods, surface chemistry is also favorable for activating the HER activities of MTMCs. Our group proposed several approaches for improving the HER performance of Mo_2C by tuning the surface properties [101,103]. Such as, we designed monolayered 2D Mo_2C nanosheets with various dopants to improve the wettability properties, as shown in Fig. 6a. The hydrophilic nitrogen and sulfur-doping resulted in greatly increased electrolyte–electrode contact points, favoring the electron transfer between the 2D Mo_2C nanosheets and the redox species. The adjacent N–S pair doped in Mo_2C also significantly improved the reaction kinetics through electron-acceptor and electron-donor interactions (Fig. 6d). As such, a low operating potential with -86 mV at -10 mA cm^{-2} was achieved (Fig. 6b-c).

In addition to HER, the MTMCs also show promising application for ORR. For example, Guo and co-workers developed ultrasmall WC clusters encapsulated in high-defective graphitic layers for electrocatalytic ORR with both remarkable activity (4-electron transfer) and stability (~80% activity retention after 30,000 s) in 0.1 M KOH electrolyte [137]. Due to the D-electrons positioned both at external corners and edges of unsaturated W atoms, such sub-nanometer WC clusters showed much increased density of states near the Fermi surface and improved ORR activity, as verified theoretical simulation by DFT calculation. Furthermore, the as-wrapped graphitic layers accelerated the transportation of ions and electrons, accompanying with decreasing the chemical/thermal corrosion of WC catalysts. These combined advantages resulted in the greatly improved electrocatalytic activity and stability. The ORR performance of MTMCs are also related to their metal composition. Normally, the MTMCs with two or more metals show better ORR activity than the single-metal counterpart owing to the synergistic functions resulting from charge transfer between each components; thus, enhancing the surface strain and active sites [91,139,140]. For instance, Gautam and co-workers recently reported the preparation of cobalt iron carbide nanoparticles enwrapped by N-doped graphene as highly efficient ORR electrocatalyst through an easy refluxing method followed by a post sintering process [91]. Such bimetallic carbide followed 4-electron reaction process accompanying with good diffusion limit current density, remarkable onset potential (−40 mV) and half-wave potential (−110 mV). Additionally, coupled with the unique mesoporous structure, the high interactions between two Co and Fe enable the hybrid electrocatalysts with superior stability (~96.2% activity retention after 12000s) and exceptional methanol tolerance (no noticeable change in activity) compared to Pt/C. The above studies provide numerous effective guidelines for the design of various high performance electrocatalysts based on MTMCs.

Compared to HER and ORR, there are less interest focused on developing MTMCs for electrocatalytic OER. Among the few studies, cobalt and molybdenum-based MTMCs have attracted the most attention [87,131]. Tang et al., found that the Co/Mo molar ratio is of critical significance to electrocatalytic OER performance. The optimized $Co_6Mo_6C_2$ exhibits an overpotential of 260 mV at 10 mA cm^{-2} and a Tafel slope of 50 mV dec^{-1} [87]. A optimized composite of nitrogen-doped carbon encapsulating cobalt and molybdenum carbide nanoparticles (Co_xMo_y@NC) developed by Jiang and co-workers also afforded 10 mA cm^{-2} at an overpotential of 330 mV with a Tafel slope of 48.7 mV dec^{-1} [131].

Nitrides

Nitrogen is the most abundant component of the earth's atmosphere. Similar to its neighbors, which are carbon and phosphorus, nitrogen can form metallic transition metal nitrides (MTMNs) with almost all of the transition metals. With regards to the com-

mon close package lattices including face-centered cubic (fcc) and hexagonal close-packed (hcp) of transition metal atoms, the MTMNs crystal structure, similar to that of MTMCs, can be considered as an interstitial alloy of nitrogen atoms in transition metal lattices. With the intercalation of nitrogen atoms, the distance between metal atoms is expanded. But the MTMNs with general formulae of MN, M_2N, and M_4N can still maintain cubic or hcp structure [141]. The MTMNs are well known for their high conductivity, refractoriness, and hardness. These properties make the MTMNs especially suited for crucibles, thermocouple sheaths, and cutter coating. Interestingly, the applications of some MTMNs in heterogeneous catalytic reactions are discovered in the last century. For instance, iron nitrides as Fischer-Tropsch catalysts [142]. In addition, it was found that the nitrogen can replace carbon atoms in most of the MTMCs, forming the substitutional solid solution (N-doped MTMCs, so called MTMCNs). In regard to the widely studies and application of MTMNs and MTMCNs; herein, we offer a brief summary of recent advances on the synthesis and applications of MTMNs in energy storage and conversion. The representative works in this field will be discussed in detail to give an in-depth understanding.

Synthesis of MTMNs

Conventionally, MTMNs are also prepared by CVD) or PVD techniques, in which the MTMNs thin film can be prepared from metal halides or metal organic precursors (such as $TICl_4$, $[W(NtBu)_2(NMe_2)\{(iPrN)_2CNMe_2\}]$ and $[W(NtBu)_2(H)\{(iPrN)_2CNMe_2\}]$)by the direct pyrolysis reaction or evaporation/sputtering methods [143–145]. However, direct deposition of MTMNs through CVD and PVD methods usually results in condensed products. For the application of energy storage and conversion, the materials are required to be porous, which can offer enough path for the transportation of charge carriers in the electrolyte and large surface for reactions. Therefore, alternative synthesis methods were required to obtain MTMNs nanostructures.

During the past decade, the most common method to prepare MTMNs nanostructures is via ammonolysis reaction where metal oxide precursors are nitrided in NH_3 atmosphere at high temperature ($M_xO_y + NH_3 \rightarrow MN + H_2O$ at 600–800 °C). Similar to PH_3 route for MTMPs synthesis, the synthesized MTMNs would inherit the nanostructures of the metal precursors [146–148]. In addition, this method allows the synthesis to be done at a lower temperature and pressure as compared to the conventional method that uses Ns gas as the nitrogen source ($M + N_2 \rightarrow MN$), in which the N≡N bonds is hard to break down (requires 945 kJ mol^{-1}) [149–151]. Beyond this, recently, another method involved N_2 RF-plasma treatment was introduced to synthesize $Ni_{0.2}Mo_{0.8}N$ film at a lower reaction temperature of 450 °C and shorter duration of 10–15 minutes (compared to the lowest of 600–800 °C for few hours by the NH_3 route) [147]. As there are various excited N_2, N_2^+ and N species in the N_2 RF-plasma, with which the Ni and Mo atoms would easily react during the sputtering process, resulting in the recrystallization of $Ni_{0.2}Mo_{0.8}N$ phase from NiMo alloy film. This facile, effective, and environmentally benign method was quickly becoming a major focus for the synthesis of MTMNs, and a comprehensive review on this method was published last year [152]. However, this ammonolysis method suffers from the hazardousness of NH_3 and the difficulty to have complete nitridation.

Besides, the precursors contain amine or other nitrogen-contained species are also can directly transform into MTMNs through the pyrolysis process [153,154]. Among these nitrogen-contained species, urea was one of the most economic nitrogen sources. Therefore, the pyrolysis of urea-contained precursor named “urea glass route” has been widely studied CrN, VN, Mo_2N, NbN, W_2N, and TiN [155,156]. In this method, metal chlorides need to be reactive with ethanol to obtain metal orthoester gels (and release HCl) after which appropriate amount of urea is added. Subsequent pyrolysis under N_2 at around 800 °C would transform the gels to MTMNs ($MCl_x + CO(NH_2)_2 \rightarrow MN + CO + HCl$). Still based on this versatile route, Dai et al. recently has developed a strategy to obtain high-entropy MTMNs, by which instead of reacting with ethanol, the transition metal chlorides and urea were ball-milled to form a metal-urea gel which was then annealed in N_2 atmosphere (Fig. 7a-l) [157].

Applications of MTMNs

When turning to the application of MTMNs in the fields of energy storage and conversion, it should be pointed out that the high conductivity of MTMNs endows them great potential in these fields, similar to MTMPs and MTMCs. However, some of the MTMNs (such as TiN and WN) are usually suffered from their low capability when exposed to water or oxygen atmosphere, which is originated from the irreversible electrochemical oxidation [158,159]. In addition, when applied to LIBs, although the Li_3N product provides much higher theoretical capacity, the conversion of MN into elemental M and Li_3N will lead to the pulverization of MN nanostructure, resulting in poor cycling and rate performance [114,160–165]. In this section, we focus on the recent progress on how to design and synthesize stable MTMNs nanostructures for energy storage and electrocatalytic applications.

Electrode materials (Supercapacitors and Batteries)

For the energy storage devices such as LIBs/SIBs, very much similar to MTMPs, the MTMNs are usually undergo a conversion reaction, the general reaction mechanism can be expressed as: $3M_xN_y + 3yLi^+$ (or Na^+) $+ 3ye^- \rightarrow xM + yLi_3N$ (or yNa_3N). However, although the conversion mechanism can offer a high theoretical specific capacity (~300 mA h g^{-1} for TiN in case of LIBs) [160], the volume change during cycling process will result in the pulverization of electrode and the rapid capacity decay, which is the main obstacle for the further application of MTMNs.

In order to enhance the cycling and rate performance, Tong et al. recently reported a 3D Ni_3N/carbon cloth (CC) composite obtained by nitridation of nickel hydroxide under ammonia atmosphere [166]. The Ni_3N nanosheets grown on CC consist of small particles with an average size of tens of nanometers. It was believed that the diffusivity of Li-ion in the material could be effectively promoted by reducing the characteristic dimensions of MTMNs particles. As a result, the 3D Ni_3N/CC composite delivered a reversible capacity of 593 mA h g^{-1} at 1 C. With increasing current densities, the composite still achieved a reversible capacity retention of over 50% at 10 C (304 mA h g^{-1}) (Fig. 8a-d). This strategy of incorporating MTMNs (WN nanowires, TiN nanowires, etc.) into 3D structure to enhance the diffusivity of lithium ion was also reported by a number of groups [160,162].

By applying the recent-developed plasma-active method, Fan and Rawat synthesized a hierarchical Ni_3N nanocoral covered by graphene quantum dots (GQD@hNi_3N) for Li-ion storage [167]. The Ni_3N@hNi_3N nanocoral was obtained by a simple N_2 RF-plasma treatment of nickel foam, followed by electrolytic deposition of GQDs. The reversible capacity of this nanocoral was 450 mA h g^{-1} at the current density of around 1 C after 500 cycles. Though the maximum capacity of GQD@hNi_3N was lower than that of the 3D Ni_3N/CC composite reported by Tong et al., the cycle stability of GQD@hNi_3N improved significantly. This might be because the GQDs layer can facilitate the transfer of Li-ion and form a stable SEI film.

Another way designing and constructing nanostructured MTMN electrodes to suppress the volume changes after long cycling was

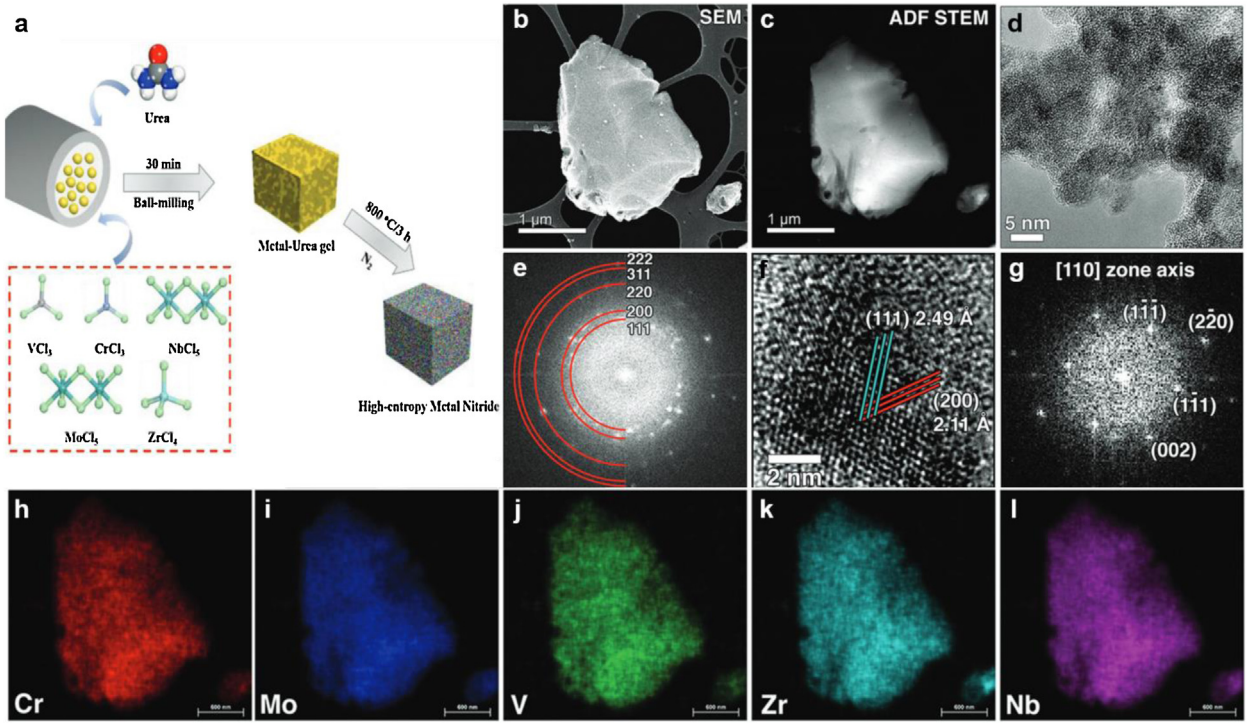

Fig. 7. (a) Synthetic strategy for high-entropy metal nitride. (b) SEM images and (c) ADF STEM image of HEMN-1. (d) HRTEM image and (e) its corresponding FFT pattern. (f) HRTEM image from an individual grain and (g) its corresponding FFT pattern aligned along the [110] zone axis. (h–l) EDS elemental mapping of (h) Cr, (i) Mo, (*j*) V, (k) Zr, and (l) Nb. Reproduced with permission from [157] Copyright 2018, Wiley-VCH.

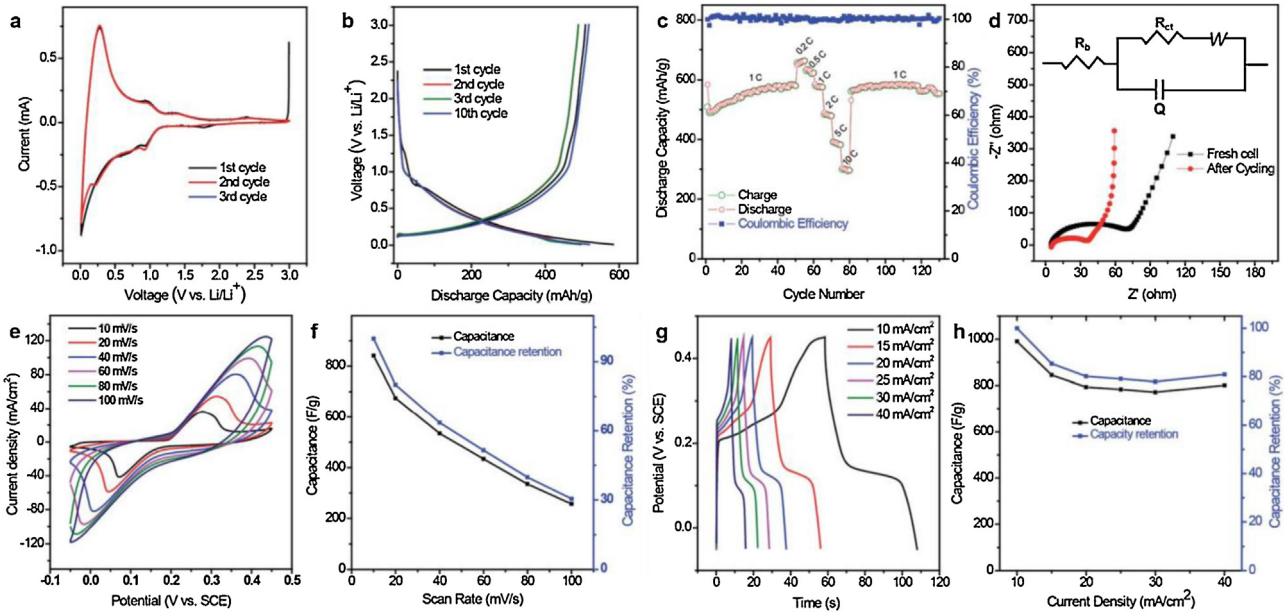

Fig. 8. (a–d) Lithium storage performance. (a) CV curves, (b) charge– discharge profiles, (c) rate performance, (d) Nyquist plot of the 3D Ni_3N/carbon cloth composite electrode (Inset: equivalent circuit). (e–h) Supercapacitor performance. (e) CV curves, (f) areal capacitance measured vs. scan rate, (g) galvanostatic charge/ discharge curves collected at 40 mA cm^{-2}, (h) specific capacitance vs. current density of the 3D Ni_3N/ carbon cloth composite electrode. Reproduced with permission from [166] Copyright 2016, Royal Society of Chemistry.

reported by Jin et al. [164] In this work, the nanostructured porous Fe_2N encapsulated in carbon microboxes (Fe_2N@C) was synthesized via an innovative ammonolysis of polymer coated Fe_2O_3 microcubes. The carbon microboxes helped to secure the core Fe_2N from oxidation and keep a thin, stable SEI layer. In addition, the sufficient voids in the Fe2N cubes guaranteed there is less volume expansion during charge/discharge processes. Concretely, by measuring the thickness of the both electrodes Fe_2N and Fe_2N@C before and after lithiation; the Fe_2N@C indicated only 9̃% change in volume while the as-synthesized Fe2N showed 90% increase in volume. Consequently, the Fe_2N@C anode demonstrated superior volumetric capacity of 1030 mA h cm^{-3} and excellent cycling performance with 91% capacity retention after 2500 cycles at as high current density as 10 A g^{-1}.Supercapacitor is another kind of energy

storage device with high power density [168–173]. In Tong's work, the 3D Ni_3N/CC composite was also tested as electrode for supercapacitor. The composite showed pseudocapacitances of 990, 845, 793, 783, 771 and 800 F g^{-1} at 10, 15, 20, 25, 30 and 40 mA cm^{-2}, respectively (Fig. 8e-h) [166]. Fan's group also reported a Fe_2N-Ti_2N (FTN) core-shell nanorod array electrodes for supercapacitive device [148]. The supercapacitor displays a steady working voltage of 2.0 V with high capacitance of $\tilde{8}6$ F g^{-1} at 2.7 A g^{-1}, which could be maintained for more than 20,000 cycles. Recently, Dai et al. reported a novel high-entropy MTMNs for supercapacitive devices [157]. However, there are still lack of in-depth research about the energy-storage mechanism of MTMNs for supercapacitors.

Electrocatalysts (HER, OER, and ORR)

The studies of MTMNs in the application of electrocatalytic HER, OER, and ORR have emerged over several decades [174–180]. It was confirmed that with their good conductivity, activity, and selectivity, MTMNs are promising superior electrocatalysts with comparable activity to noble metals [142,174,181–184].

For HER application, the surface metal M–H binding plays a critical role on the catalytic activities. Traditionally, the Ni_3N has been widely evaluated as an effective catalyst for HER process [183]. However, the Ni-H binding is relatively weak, which hamper the further improvement of HER activities. Rawat and Fan recently employed the strategy of heteroatom incorporation into metal nitrides and studied the HER performance of a 3D hierarchical porous nickel-molybdenum nitride (NiMoN) obtained by the innovative N_2 RF-plasma treatment of nickel-molybdenum alloy [147]. The plasma-treated NiMoN showed a coral-like structure, which might be originated from the recrystallization of metal nitride species. As compared to Ni_3N, which required an overpotential of 208 mV at -10 mA cm^{-2} in the 1.0 M KOH solution, the NiMoN only needed 109 mV. In consideration of the HER performance enhancement, the 3D hierarchical porous structure and the synergy between weak Ni-H binding energy and strong Mo-H binding energy provided a valuable guidance towards the design of high-efficiency MTMNs HER electrocatalyst.

Besides outstanding conductivity, some of the MTMNs (like WN) are also known for their exceptional corrosion resistivity in acidic condition. However, they still show poor performance towards HER. Until recently, Shao et al. designed a WN_x/nitrogen-rich porous graphene-like carbon (NRPGC) composite, which combined the advantages of both WN_x and NRPGC [185]. That is, the pyrolysis process suppressed the growth of WNx nanoparticles, creating more available active sites for HER; in addition, the graphene-like carbon endowed the rapid electron transfer pathway. In comparison with the bulk WN that showed an overpotential of 492 mV, the as-derived WN_x-NRPGC catalyst showed a great improvement of HER performance, which required only -132 mV to drive -10 mA cm^{-2} in 0.5 M H_2SO_4 solution.

Another material design strategy is to confine the MTMNs nanoparticles in a conductive framework, in which the electron can immigrate freely even in case of the damaged catalyst surface. Wu and the co-workers recently reported a cobalt nitride-based electrocatalyst [186]. The $Co_{5.47}N$ nanoparticle was encapsulated in a 3D N-doped porous carbon ($Co_{5.47}N$ NP@N-PC), which was synthesized by directly annealed Co-ZIF-67 in an ammonia atmosphere. When evaluated as an electrocatalyst for HER reaction, the $Co_{5.47}N$ NP@N-PC reached -10 mA cm^{-2} in 1.0 M KOH with an overpotentials of only 149 mV.

As for the OER application, Ouyang et al. also reported the OER activity of a nitrogen-plasma-treated hierarchical Ni_3N (hNi_3N) nanocorals on Ni foam. Although the hNi_3N is grown on a conductive Ni foam and possessed a corals-like nanostructure, it still revealed an overpotential of 325 mV at 10 mA cm^{-2} in 1.0 M KOH solution [167]. Similar to MTMPs, this unsatisfied performance might be due to the fact that the real OER active sites of MTMNs, which are the in-situ surface-generated poor electrical conductivity metal hydroxides/oxyhydroxides, also plays as an insulating layer hindering electron transport [70,187–191]. While in another work, Vaidhyanathan et al. reported a benzimidazole covalent organic frameworks (COFs) supported Ni_3N catalyst, in which the Ni_3N catalyst with a crystal size < 2 nm was restricted in the channels of the COF [192]. In this form, the porous COF support could restrict the exposed surface of Ni_3N nanoparticles and offered a higher active surface area. As a result, the Ni_3N@COF composite showed an OER overpotential of 230 mV at 10 mA cm^{-2} in 1.0 M KOH, which was about a 100 mV lower than the plasma-treated hNi_3N nanocorals. These works indicate that in order to realize the high-efficiency OER catalysis, the MTMNs might need to be increased the active surface area while restricting the thickness of the surface oxide layer.

The $Co_{5.47}N$ NP@N-PC were also evaluated as an OER catalyst by Wu and the co-workers [186]. The $Co_{5.47}N$ NP@N-PC reached 10 mA cm^{-2} in 1.0 M KOH with overpotentials of 248 mV. By evaluated the turnover frequencies (TOFs) and charge-transfer resistance of $Co_{5.47}N$ NP@N-PC and Co NP@N-PC, it was concluded that the high electrocatalytic water splitting performance is related to the rich active sites and fast charge transport character in the $Co_{5.47}N$ NP@N-PC.

Beyond HER and OER applications, the ORR is also an important electrocatalytic process in fuel cell. In consideration of the cost-efficiency and potential activities of MTMNs, they have received increasing interest in recent years. Siahrostami et al. had studied the ORR catalytic actives of cobalt nitride (CoN) by DFT calculation [193]. After comparing the interaction energies of various intermediates on different facets of CoN, the authors demonstrated that the surface oxidation layer on CoN could reduce the ORR overpotential significantly. Especially, the (111) facet of zinc blend phase cobalt nitride (CoN_{ZB}) with a single surface CoO layer was the most active facet for the ORR process. Titanium nitride (TiN) was another promising ORR catalyst to replace precious metals [141]. However, the efficient electron transport in TiN required a proper design of morphology and particle size. For this reason, Liao and Song had designed a 3D nitrogen-doped carbon-coated hierarchical $Ti_{0.95}Co_{0.05}N$ composite [194]. The as-obtained $Ti_{0.95}Co_{0.05}N$ catalyst showed a significant enhancement of ORR activity. This might be ascribed to the synergism of Co doping and surface nitrogen-doped carbon coating, which resulted in a higher surface area and offered better mass and electron transfer. As a result, the optimal $Ti_{0.95}Co_{0.05}N$ catalyst with 20% C presented almost comparable ORR performance to 20% Pt/C in 1.0 M KOH.

Borides

Compared to transition metal carbides, nitrides and phosphides, transition metal borides (TMBs) are less well explored for energy storage and conversion applications. Similar to metal phosphides/nitrides, boron can form borides with most of the transition metals [195]. Most of TMBs share (M – B) bonds with a strong covalent component. These bonds are normally stronger than those seen in TMCs and TMNs. With increasing boron content, TMB compounds display numerous compositions (from M_3B to MB_{66}) with the character from metallic to semiconducting state. Among those, metallic TMBs (MTMBs) with unique properties, just like those MLTMNs discussed above, has attracted more attention [12,196]. In addition to the character of hardness, MTMBs also show a variety of interesting electronic ground states, including superconductivity and high chemical and thermal stability [197–200]. In this section, we summarize the typical synthesis methods and recent progress of MTMBs for energy applications.

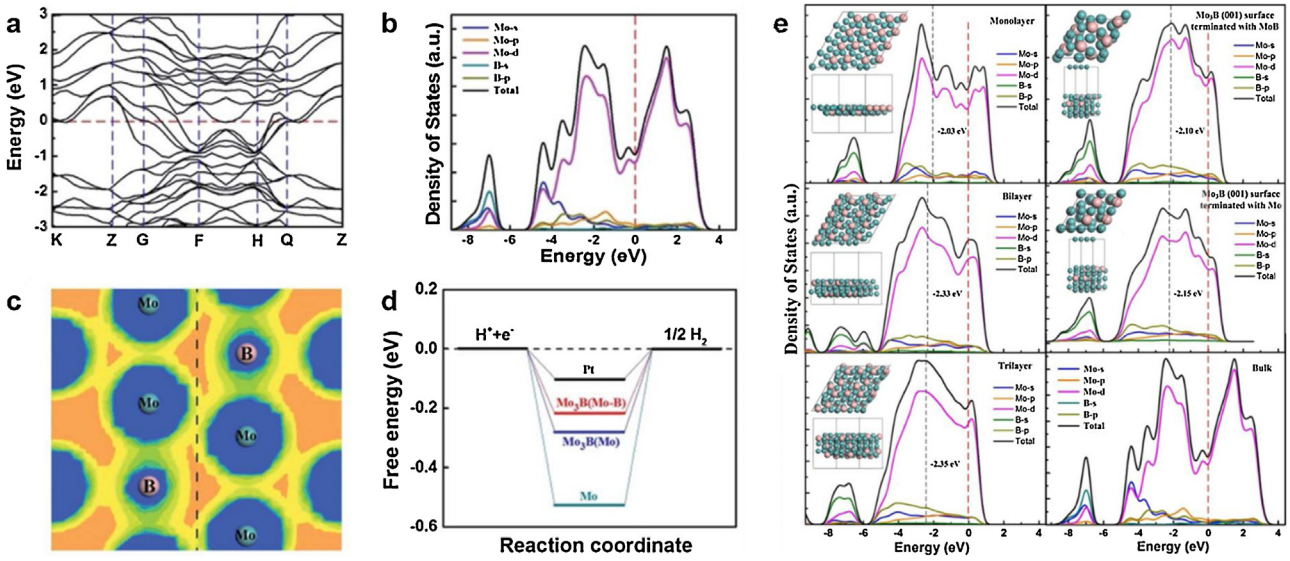

Fig. 9. First-principles calculations of the electronic properties of the Mo_3B thin film. (a) electronic band structure of the Mo_3B thin film (red dashed line: Fermi level). (b) Calculated total DOS and local DOS of the Mo (s, p and d) and B (s and p). (c) Electron density map of the ultrathin Mo_3B film. (d) Free energy evolution of H during the HER catalyzed by various materials. (e) DOS patterns of mono-, bi- and tri- layer Mo_3B, its surface terminated Mo-B and Mo as well as the bulk counterpart. Reproduced with permission from [198] Copyright 2017, Royal Society of Chemistry.

Synthetic methodologies

There are lots of methods for preparing MTMBs, which has been well summarized in the literature [12]. Here, we just focus on these methods used to prepare MTMBs for energy conversion processes.

CVD methods for preparing of MTMBs can be dated back to 1970s when gaseous reactive B were used for B doping in semiconductor industry [201–203]. The CVD processes can be divided into self-catalyzed CVD and metal-catalyzed CVD process. In the self-catalyzed CVD process, the metal substrate acts as the catalysts itself and react directly with the gaseous boron sources to form metal borides [23,204,205]. Whereas, in the metal-catalyzed CVD process, an additional metal is required to serve as catalyst [206,207]. For example, the Mo_3B films were obtained through metal-catalyzed CVD process, in which the mixture of boron and boron oxide (B_2O_3) served as boron source and the metal Mo foil acts as the catalyst and growth substrate.

Other than CVD, chemical reduction of soluble transition metal salts by metal borohydrides is the most used method [208–210]. Generally, the chemical reduction process was carried out by adding the chilled reducing solution containing metal borohydrides ($NaBH_4$ or KBH_4) into the metal precursor (usually metal chlorides) aqueous solution under the argon gas atmosphere. After continuous vigorous stirring until the bubble stops, the precipitates were collected by centrifugation and washing. The proposed reaction is shown as below:

$$MCl_x + NaBH_4 + H_2O \rightarrow M_yB + NaCl + H_2 + B(OH)_3$$

With this method, the products are usually in amorphous phase. However, by a subsequent annealing step, the crystallinity can be increased, giving MB, M_2B, or M_3B or mixture of those depending on temperature and annealing duration [208,209]. For examples, Schuhmann et al. reported the transformation of Ni-B amorphous to mixture of Ni_3B as the major phase and Ni_2B as a minor phase at annealing temperature of 600 °C. Further increase of annealing temperature to 1000 °C would increase the Ni_3B content (up to 79% according to their Rietveld refinement) but Ni_2B signals were still detected [209].

Applications of MTMBs

MTMBs, such as Fe-B alloy, Co-B alloy and Mg–Co–B alloys, have been reported as electrodes for secondary alkaline batteries [211–214]. However, to the best of our knowledge, MTMBs are rarely studied as electrodes for LIBs/SIBs. Using first principles calculations, Sun *et al.* reported that by selectively etching the A layer from a family of layered transition metal borides (MAB phases), a new family of 2D transition metal borides can be obtained. Their calculation results show that Mo_2B_2 and Fe_2B_2 are metallic-like with excellent electronic conductivity and have an omnidirectional small diffusion energy barrier and high storage capacity for Li atoms, suggesting their promising application as electrode materials in LIBs [215]. Kumta et al. reported that the TiB_2 is inactive for LIBs, but it appears to increase the stability of the capacity of the nanocomposite electrodes due to a probable homogeneous distribution of the induced stress during cycling [216].

As discussed in previous sections, MTMPs, MTMCs, and MTMNs have been described to exhibit promising HER, OER, and ORR performance. This is due to the fast charge transfer between different elements, the modified electronic structures, and the lowered kinetic energy barriers of the electrochemical processes. MTMBs have the similar bonding schema to MTMPs, indicating that they should have the similar properties for electrocatalytic activities. Some studies focus on MTMBs have already shown the great potential of them for HER, OER and ORR applications.

Currently, most of reports on MTMBs as electrocatalysts for HER are on molybdenum, cobalt, and nickel borides [198,217–220]. Hu et al., reported for the first time of using polycrystalline molybdenum boride (α-MoB) for HER. In their case, the MoB nanoparticles show high activity in both acidic and alkaline conditions. At a current density of -20 mA cm^{-2}, the overpotentials for MoB at pH = 0 and pH = 14 are all located between 210–240 mV with Tafel slope of 55 mV dec^{-1} and 59 mV dec^{-1}, respectively [217]. Apart from the 0D molybdenum borides, ultrathin 2D hexagonal Mo_3B films of 6.48 nm thicknesses on Mo foils, prepared by chemical vapor deposition, exhibit the smallest Tafel slope of 52 mV dec^{-1} in acidic solution (pH = 0) among the reported molybdenum borides.

The reasons for such good HER performance was well-explained by first-principles calculations. First, the density of state (DOS) confirms the metallicity of the materials, which benefit electron transport along the active edges (Fig. 9a-b). Furthermore, there is a decrease in electron density around Mo atoms (Fig. 9c), which consequently lowers the D-band center of Mo and halves $|\Delta G_{H^*}|$ from 0.56 eV of the Mo to 0.22 eV and 0.30 eV of the Mo_3B surfaces terminated with Mo–B and Mo, respectively (Fig. 9d). They also demonstrated the importance of the thin 2D nanostructure. The thinner the nanofilms, the narrower the D-band center energies of Mo_3B, which lead to smaller $|\Delta G_{H^*}|$ (Fig. 9e) [198].

The strategy of incorporating more metal species to improve electrochemical performance applies well for MTMBs. Wang et al., reported the bi-metalic Co–Ni–B nanoparticles grown on nickel foam, in which the nanocrystallites were embedded in amorphous phase. This amorphous layer acted as a stabilizer to keep the metallic core from coarsening and oxidation. By annealing in Ar atmosphere, the annealed Co–Ni–B@NF catalyst exhibited high and stable activity toward HER in alkaline solution (pH = 14) with an overpotential of 205 mV at -10 mA cm^{-2}, which was much lower than 306 mV of single-metal $NiB_{0.54}$@Ni foil reported by Sun and co-workers [221,222].

Regarding OER, the investigation of MTMBs for OER activity is as early as the 1980s. In that report, Co- and Ni- based borides indicated favorable activity compared to other TMBs [223]. Therefore, most of the works later only focused on developing these two kinds of borides. Hu and his group reported a core–shell structure consisting of a Ni^{II}-Bi shell on a nickel boride (NB) nanoparticle core (Ni-Bi@NB). In their report, the OER activity was tuned by regulating the crystallinity of the Ni^{II}-Bi shell. At 10 mA cm^{-2}, 364 mV overpotential was needed for amorphous Ni-Bi@NB (a-Ni-B_i@NB) electrocatalyst. The number was downed significantly to 302 mV for partially crystalline one (pc-Ni-B_i@NB), which was lower than that of the commercial IrO_2 (325 mV). Further improving the crystallinity of the Ni-B_i shell would lower the activity. The higher OER performance of pc-Ni-Bi@NB was explained by the quantitative turnover frequencies (TOF) analysis in which pc-Ni-B_i@NB showed 7-fold TOF higher than that of a-Ni-B_i@NB. The Tafel slope was 52 mV dec^{-1} for partially crystalline Ni-Bi@NB [224].

Bi-metallic boride Co–*x*Ni–B was also reported for OER by Wang et al. The optimized Co–*x*Ni–B showed an overpotential of 310 mV at 10 mA cm^{-2}. Just like MTMPs and MTMNs, the facile formation of hydroxides/oxyhydroxides intermediates during the catalytic processes and a substantial increase in surface area due to the incorporation of the second metal into monometallic boride were the main contributors to the superior catalytic performance [225]. In a similar manner, Albert et al., reported the combination of Co and Fe in metallic borides. Their optimized $(Co_{0.7}Fe_{0.3})_2B$ displayed a low onset overpotential of 0.27 V in 1.0 M KOH solution with a Tafel slope of 39 mV dec^{-1}, which was comparable to that of IrO_2/RuO_2 and surpass the single metal Co_2B and Fe_2B by a great margin [210].

In respect of ORR, MTMBs are less explored. There are only a few reports up to date. For instance, Schuhmann et al., directly grew the nitrogen-doped carbon nanotubes (NCNTs) on cobalt boride (CoB) nanoparticles by CVD method. The optimized CoB/NCNT exhibited excellent activity towards OER and ORR in 0.1 M KOH solution with an overpotential of only 0.73 V between ORR (at −1 mA cm^{-2}) and OER (at 10 mA cm^{-2}). Importantly, by CoB/NCNT catalyst oxygen was reduced via 4-electron pathways other than 2-electron pathway which gives lower discharge current and facilitated H_2O_2 by-product [226]. Different from the normal understanding that the ORR activity originates from the surface of the NCNTs, they believe that the small CoB nanoparticles uniformly distributed within the NCNT could supplement ORR electrocatalysis by either playing the role as active sites or promoting the ORR via secondary effects such as modulating the chemisorption energy of molecular oxygen and the intermediates involved in the ORR.

Summary and outlook

The small addition of phosphorus, carbon, nitrogen, or boron into the host transition metals results in classes of MLTMNs with flexibility and wide scope of applications. To this end, we have comprehensively summarized and discussed MLTMNs for energy storage and conversion applications in terms of synthetic methodologies with their own advantages and disadvantages of each approach as well as strategies to improve the performance or overcome their limitations. We have also highlighted some recently break-through works for improving the efficiency of the materials in respective applications. The synthesis methods, resulting morphologies, and performances of various MLTMNs towards respective energy conversion (HER, OER) and storage (LIBs/SIBs, supercapacitors) applications are summarized in Tables 2–5. In general, considerable efforts have been made with understanding of structural characteristics, electrochemical performances, and intrinsic catalytic activity. Several advances have been made in this promising field. Due to much-improved electrode kinetics and charge transport, MLTMNs show superior electrocatalysis and energy storage performance compared to these of semiconducting/insulating counterparts which inspire researchers to attain in-depth mechanism underneath together with further optimizing the materials for even better performance. The performance of those materials has been advanced remarkably with many strategies like optimization of compositions, especially those targeting for better electrocatalysis. This has been achieved by slight modified conventional techniques or innovative processing techniques, i.e. plasma enhanced CVD, BP for phosphides synthesis, hybridized with carbon nanomaterials, etc. where important parameters involved were finely tuned.

However, the development of MLTMNs is still facing some obstacles that decelerate its progress, of which solving those would provide more guidelines for the future of this promising domain. Firstly, there is still not much of knowledge on the nature of intermediates during the synthesis which is necessary for the development of rationally designed synthesis method to produce materials that are phase-pure or with certain facet, or to control the morphology and sizes. In this regard, the blend of in-situ equipment and experimental techniques to achieve time resolution and spatial resolution measurement is urgently needed to reveal the inter/intra -molecular interaction. Moreover, modeling targeted compounds would visually give better understanding to synthesis methodology from molecular thermodynamics point of view. Additionally, not only new and innovated materials are necessary but also comprehensive mechanistic understanding at atomic/molecular level of electrochemical reactions happening in batteries, supercapacitors, and electrocatalysis. Catalytic behavior at the surface/interface during operation can be monitored via in situ HRTEM, EXAFS, etc. Many fundamental problems are still there, namely, precise capture of reaction intermediates or charge/discharge products, interface characteristics. By these in-depth investigations, rationally designed materials and optimization of their performance are more feasible. Last but not least, the practical feasibility of the materials should be taken into account. There is currently a huge gap between fundamental research of MLTMNs and their practical applications toward energy storage and conversion. The materials synthesized should be judged for feasibility in industrial scale. Facile, scalable and sustainable synthesis and milder reaction conditions for industrial needs should be taken into consideration, especially in the case of carbides. The development in synthetic methodologies and engineering may possibly resolve the

Table 2
Summary of the HER performances of MLTMNs synthesized via various methods.

Material and morphology	Synthesis method	Electrolytes	Substrate	Mass loading (mg cm^{-2})	η_{10} (mV)	Tafel slope (mV dec^{-1})	j_0 (mA cm^{-2})	Ref.
$Ni_{12}P_5$ nanoparticles	TOP route	0.5 M H_2SO_4	Ti foil	3	143 @ -20 mA cm^{-2}	63	n.a.	[15]
Ni_5P_4 nanoparticles	TOP route	1 M H_2SO_4	Self-standing	29	62 @ -100 mA cm^{-2}	33	0.96	[16]
FeP nanoparticles	TOP route	0.5 M H_2SO_4	Ti foil	1	50	37	0.43	[18]
Ni_2P hollow nanoparticles	TOP route	0.5 M H_2SO_4	Ti foil	1	130 @ -20 mA cm^{-2}	~46	0.49	[19]
Co_2P hollow nanoparticles	TOP route	0.5 M H_2SO_4	Ti foil	1	95	45	n.a.	[21]
CoP hollow nanoparticles	TOP route	0.5 M H_2SO_4	Ti foil	1	75	50	n.a.	[21]
		0.5 M H_2SO_4				68		
Ni_2P nanosheets	TOP route	0.5 M PBS	NF	7.2	n.a	142	n.a	[74]
		1 M KOH				50		
MoP @ porous honeycomb carbon	Phosphate route	0.5 M H_2SO_4	GCE	n.a	129	48	n.a.	[65]
Ni_2P nanoparticles@BP	Elemental P route	0.5 M H_2SO_4	GCE	n.a	107	38.6	n.a	[36]
BP/Co_2P nanoparticles	Elemental P route	0.5 M H_2SO_4	GCE	n.a	336 @ -100 mA cm^{-2}	62	n.a	[38]
		1 M KOH			340 @ -100 mA cm^{-2}	72		
WP nanorod arrays	Elemental P route	0.5 M H_2SO_4	CC	n.a	130	69	0.29	[66]
Ni-P nanosheets	Elemental P route	0.5 M H_2SO_4	CP	25.8	162	58.8	0.24	[72]
		1 M KOH			250	85.4	n.a.	
MoP nanoparticles@C	PH_3 route	0.5 M H_2SO_4	CC	6	88	50.4	n.a.	[6]
		1 M KOH			49	54	0.69	
NiCoP nanosheets	Plasma-assisted PH_3 route	1 M KOH	NF	n.a	32	37	1.36	[40]
$NiMoP_2$ nanowire	PH_3 route	0.5 M H_2SO_4	CC	5	195 @ -100 mA cm^{-2}	56	n.a	[44]
O_2 plasma treated CoP nanowire	PH_3 route	1 M KOH	CC	n.a	n.a	42.8	n.a.	[63]
		0.5 M H_2SO_4			74	50	0.518	
N, P doped carbon-encapsulated MoP nanocrystal	PH_3 route	1 M PBS	CC	2.42	106	52	n.a	[64]
		1 M KOH			69	73	0.706	
FeP nanorod arrays	PH_3 route	0.5 M H_2SO_4	CC	1.5	58	45	0.5	[71]
		0.5 M H_2SO_4			67	51		
CoP nanowire arrays	PH_3 route	1 M PBS	CC	0.92	106	93	0.288	[73]
		1 M KOH			209	129		
CoP nanocrystal/CNT	PH_3 route	0.5 M H_2SO_4	GCE	0.285	122	54	0.13	[76]
$NiCoFe_xP$ nanosheets	PH_3 route	1 M KOH	CC	2	39	50	n.a	[77]
Oxygen plasma treated V-Ni_2P nanosheets	PH_3 route	1 M KOH	GCE	n.a	108	72.3	n.a	[78]
		0.5 M H_2SO_4			135	62		
MoC_x nanoparticles encapsulated in N,S-doped graphene	carbothermal	0.2 M PBS	GCE	0.45	165	105	n.a	[130]
		1 M NaOH			150	99		
		0.5 M H_2SO_4			154	65		
WC_x nanoparticles encapsulated in N,S-doped graphene	carbothermal	0.2 M PBS	GCE	0.45	220	115	n.a	[130]
		1 M NaOH			262	115		
Mo_2C nanoparticles on rGO	carbothermal	0.5 M H_2SO_4	GCE	0.196	280 @ -5 mA cm^{-2}	134	n.a	[90].
N,S doped-Mo_2C nanosheets	carbothermal	0.5 M H_2SO_4	GCE	n.a	86	47	0.035	[101]
3D Hierarchical Porous Mo_2C	carbothermal	0.5 M H_2SO_4	GCE	n.a	97	60	0.28	[103]
W_2C@WC films	carbothermal	0.5 M H_2SO_4	GCE	2.7	310	108	n.a	[127]
Mo_2C nanoparticles-Graphene	carbothermal	0.5 M H_2SO_4	GCE	0.8	150	57	2.58 x10^{-2}	[127]
in-plane WC–graphene heterostructure (i-WC–G)	CVD	0.5 M H_2SO_4	Ga–W foil	–0.00222	120	38	n.a	[94]
		0.1 M KOH			225	108		
Fe-doped Ni_3C nanodots encapsulated in N-doped carbon	carbonization	1 M KOH	GCE	n.a	292	41.3	n.a	[138]
Co_2C nanoparticles	wet-chemistry	0.5 M H_2SO_4	GCE	n.a	181	89	n.a	[128]
Ni_3N nanoparticles	Plasma-assisted ammonolysis	1 M KOH	CC	1.1	208	113	0.12	[147]
3D hierarchical porous (NiMoN) coral-like	Plasma-assisted ammonolysis	1 M KOH	CC	1.1	109	95	0.92	[147]
WN_x/N-rich porous graphene-like carbon	Ammonolysis	0.5 M H_2SO_4	GCE	0.362	132	86	0.37	[185]
$Co_{5.47}N$ nanoparticle encapsulated in a 3D N-doped carbon	Ammonolysis	1 M KOH	GCE	n.a	149	86	n.a	[186]
α-MoB	n.a	0.5 M H_2SO_4	GCE	n.a	210-240 @ -20 mA cm^{-2}	55	1.4×10^{-3}	[217]
		1 M KOH				59	2.0×10^{-3}	
Mo_3B films	CVD	0.5 M H_2SO_4	Free-standing	n.a	249 @ -20 mA cm^{-2}	52	n.a	[198]
Co–Ni–B nanoparticles@NF	$NaBH_4$	1 M KOH	NF	n.a	205	n.a	n.a	[221]
		0.5 M H_2SO_4			45	43	0.380	
$NiB_{0.54}$@Ni nanoparticles	$NaBH_4$	1 M PBS	Cu foil	1.4	54	77	0.851	[222]
		1 M KOH			135	88	0.275	

Abbreviations are as followsNF = Ni foam, CC = Carbon cloth, CP = Carbon paper, GCE = Glassy carbon electrode, CNT = carbon nanotubes, rGO = reduced graphene oxide, η_{10} = overpotential at the current density of 10 mA cm^{-2}; j_0 = exchange current density; n.a: represents that the corresponding data are not provided in the papers cited.

Table 3
Summary of the OER performances of MLTMNs synthesized via various methods.

Material and morphology	Synthesis method	Electrolytes	Substrate	Mass loading (mg/cm^2)	η_{10} (mV)	Tafel slope (mV dec^{-1})	Ref.
NiCoP nanosheets	Plasma-assisted PH_3 route	1 M KOH	NF	n.a	330	87	[40]
Cu_3P	PH_3 route	1 M KOH	NF	n.a	290	84	[67]
$NiCoFe_xP$ nanosheets	PH_3 route	1 M KOH	CC	2	275 @ 50 mA cm^{-2}	56	[77]
NiCoP nanosheets	PH_3 route	1 M KOH	CC	2	346 @ 50 mA cm^{-2}	121	[77]
CoFeP nanosheets	PH_3 route	1 M KOH	CC	2	389 @ 50 mA cm^{-2}	137	[77]
NiFeP nanosheets	PH_3 route	1 M KOH	CC	2	425 @ 50 mA cm^{-2}	147	[77]
Oxygen plasma treated V-Ni_2P NSs	PH_3 route	1 M KOH	GCE	n.a	257	43.5	[78]
CoP and defective carbon (CoP–DC)	Elemental P route	0.1 M KOH	GCE	0.357	320	52.5	[68]
Ni-P nanosheets	Elemental P route	1 M KOH	CP	25.8	300 @ 53.8 mA cm^{-2}	73	[72]
Fe-doped Ni_3C nanodots encapsulated in N-doped carbon	carbonization	1 M KOH	GCE	n.a	275	62	[138]
$Co_6Mo_6C_2$	hydrothermal	1 M KOH	GCE	0.14	260	50	[87]
N-doped carbon encapsulating cobalt and molybdenum carbide nanoparticles	carbothermal	1 M KOH	GCE	n.a	330	48.7	[131]
Mo_2C nanoparticles supported on carbon sheets	carbothermal	1 M KOH	GCE	0.4	320	95	[132]
Co_3ZnC/Co nanojunctions encapsulated in N doped graphene	Decomposition of single source	1 M KOH	GCE	0.344	366	81	[134]
Ni/Mo_xC nanoparticle-supported N-doped graphene/CNT	carbothermal	1 M KOH	GCE	0.86	328	74	[133]
hierarchical Ni_3N (hNi_3N) nanocorals	Plasma-assisted ammonolysis	1 M KOH	NF	n.a	325	50	[167]
$Co_{5.47}N$ nanoparticle encapsulated in a 3D N-doped carbon	Ammonolysis	1 M KOH	GCE	n.a	248	86	[186]
benzimidazole COF supported Ni_3N	Urea-glass route	1 M KOH	GCE	5 μg	230	79	[192]
Fe_2Ni_2N nanoplates	Ammonolysis	1 M KOH	NF	n.a	180	34	[175]
Nanoparticle-stacked porous Co_3FeN_x nanowires	Ammonolysis	1 M KOH	NF	n.a	222 @ 20 mA cm^{-2}	46	[176]
CoN nanowires	Plasma-assisted ammonolysis	1 M KOH	NF	n.a	290	70	[177]
Ni–Mo nitride nanotubes	Ammonolysis	1 M KOH	CP	3.5	295	94	[178]
iron nitride (Fe_3N/Fe_4N) nanoporous film on graphene	Ammonolysis	1 M KOH	NF	4	238	44.5	[179]
Mn_3N_2 nanoparticles	Ammonolysis	1 M KOH	NF	3	270	97	[180]
$(Co_{0.7}Fe_{0.3})_2B$ nanoparticles	$NaBH_4$	1 M KOH	GCE	n.a	330	39	[210]
Co_2B nanoparticles	$NaBH_4$	1 M KOH	GCE	n.a	n.a	63	[210]
pc-Ni-B_i@NB nanoparticles	$NaBH_4$	1 M KOH	GCE	0.3	302	52	[224]
Co–*x*Ni–B nanoparticles	$NaBH_4$	1 M KOH	GCE	n.a	330	66	[225]

Abbreviations are as follows: NF = Ni foam, CC = Carbon cloth, CP = Carbon paper, GCE = Glassy carbon electrode, CNT = carbon nanotubes, COF = covalent organic frameworks, η_{10} = overpotential at the current density of 10 mA cm^{-2}; n.a: represents that the corresponding data are not provided in the papers cited.

Table 4
Summary of the LIBs/SIBs performances of MLTMNs synthesized via various methods.

Material and morphology	Apps	Synthesis method	Specific capacity (mA h g^{-1})	Current density (A g^{-1})	Number of cycles	Capacity retention	Ref.
yolk–shell Sn_4P_3@C nanospheres	SIBs	Elemental P route	720 505 421	0.2 C 1.5 C 3 C	400	85.5%	[51]
CoP hollow nanoparticles encapsulated in amorphous carbon	LIBs	TOP route	630 256	0.2 C 5 C	100	83.3%	[22]
Fe_2P nanoparticles enveloped in sandwich-like graphited carbon	LIBs	Phosphate route	602 362	0.1 10	200	93%	[52]
3D porous MoP @carbon hybrid	LIBs	Phosphate route	1028 384	0.1 5	500	83.8%	[53]
C@NiCoP Peapods	LIBs	Phosphate route	670 402	0.2 10	350	95%	[54]
$Ni_{12}P_5$ nanoparticles encapsulated in carbon fiber	LIBs	Phosphate route	660 388	0.1 3	200	~98%	[55]
Ni_2P nanoparticles@BP	LIBs	Elemental P route	1196.3 322	0.1 10	1000	94.1%	[36]
Sandwiched Ni_2P/C	LIBs	Hydrothermal	625 410	0.2 C 10 C	200	92.3%	[47]
Ni_3P/Ni/C nanocomposite	LIBs	Single source precursor	635	0.1	200	n.a	[48]
Peapod array of Ni_2P @ graphitized carbon on Ti substrate	LIBs	Phosphate route	634	0.2	200	97%	[49]
MoC/C nanowires	LIBs	Decomposition of single source	650.3 455.4	0.2 2	350 2000	93.4% 92%	[115]
3D porous Mo_xC@N-C with Mo vacancies	LIBs	Carbonization	825.3 266.6	0.5 5.0	200	61.9%	[112]
Mo_2C/N-doped carbon hierarchical nanowires	SIBs	Decomposition of single source	381 308	0.05 0.2	100	53.9%	[116]
MoC ultrafine nanoparticles in graphitic carbon	LIBs SIBs	Decomposition of single source	742 543.7 273.4 183.7	0.2 1 0.05 0.2	50 50	91% 62% 83% 68%	[119]
3D interconnected TiC nanoparticle chain	LIBs	Carbothermal	450 137	0.1 20	8000	92%	[92]
$MoC_{0.654}$@N-doped graphitic carbon nanosheets	LIBs	Carbothermal	1010 495	0.2 5	680	98%	[111]
3D Ni_3N/CC [a]	LIBs	Ammonolysis	593 304	1 C 10 C	250	50% at 10 C	[166]
Ni_3N@hNi_3N nanocoral	LIBs	Plasma-assisted ammonolysis	450	1 C	500	n.a	[167]
Ni_3N–Co_3N nanoparticles on CNTs [b]	LIBs	Ammonolysis	777.59 534	0.4 1.2	600	71.1%	[161]
WN nanowires	LIBs	Annealing under N_2	400	0.2	100	> 90%	[162]
TiN nanowires	Flexible LIBs	Ammonolysis	567	0.335	100	80%	[160]
Fe_2N nanoparticles	Flexible LIBs	Ammonolysis	900	6	300	76%	[163]
Carbon coated Fe_2N nanocubes	LIBs	Ammonolysis	1295 356	0.1 10	2500	> 91%	[164]
2D–0D Graphene–VN Quantum Dots	LIBs SIBs	Ammonolysis	715 201 237 149	0.24 24 0.2 C 5 C	800 800	~100% ~100%	[165]
Mo_2N nanolayer coated MoO_2 hollow nanostructures	LIBs	Ammonolysis	815 415	0.1 5	100	91%	[114]

[a] CC = Carbon cloth, [b] CNT = carbon nanotubes; n.a: represents that the corresponding data are not provided in the papers cited.

Table 5
Summary of the supercapacitor performances of MLTMNs synthesized via various methods.

	Material and morphology	Synthesis method	Reference electrode	Electrolyte	Capacitance	No. of cycles	capacitance retention	Voltage window	Ref.
MTMPs	Ni_2P nanoparticles grown on reduced graphene oxide	PH_3	Hg/HgO	2 M KOH	2266 F g^{-1} at 5 mA cm^{-2}	2500	Ĩ00%	0–0.55 V	[59]
	Ni-coated Ni_2P nanoparticles	electroless plating	Hg/HgO	2 M LiOH	1115 F g^{-1} at 2 A g^{-1}	3000	92.3%	0–0.7 V	[60]
	Ni foam supported Ni_2P nanosheet	PH_3	SCE	6 M KOH	1109 F g^{-1} at 83.3 A g^{-1}	5000	91.3%	0–1.4 V.	[61]
	Co_2P nanoflowers	TOP route	Hg/HgO	6 M KOH	416 F g^{-1} at 1.0 A g^{-1}	600	97%	−0.2 to 0.5 V	[17]
	Co_2P nanorods	TOP route	Hg/HgO	6 M KOH	284 F g^{-1} at 1.0 A g^{-1}	n.a	n.a	n.a	[17]
	Ni_2P nanoparticles on graphene sheets	PH_3 route	Hg/HgO	3 M KOH	1912 F g^{-1} at 5 mA cm^{-2}	2500	77.1%	0–0.55 V	[56]
	NiCoP nanoparticles	Elemental P route	n.a	6 M KOH	571 C g^{-1} at 1.0 A g − 1	3000	91.8%	0–0.4 V	[57]
	$Ni_{12}P_5$ nanocapsules	Elemental P route	Hg/HgO	6 M KOH	949 F g^{-1} at 1.0 A g^{-1}	2000	81%	0–0.55 V	[58]
MTMCs	3D tubular all-TiC hierarchical fibres	carbothermal	n.a	1.5 M $LiClO_4$ in ACN	185 F g^{-1} at 2.0 A g^{-1}	150,000	97%	0–1.6 V	[120]
	TaC/C nanosheets	Laser-assisted CVD	Ag/AgCl	6 M KOH	223 F g^{-1} at 1.0 A g^{-1}	5000	>94%	0.2–0.9 V	[123]
	Mo_2C incorporated onto porous carbon	carbothermal	Ag/AgCl	1 M H2SO4	750 F cm^{-3}	10,000	n.a	0.2–0.8 V	[124]
	Fe_2N-Ti_2N core-shell nanorod array	Ammonolysis	Ag/AgCl	1 M LiCl	86 F g^{-1} at 2.7 A g^{-1}	20,000	99%	0 to 2 V	[148]
MTMNs	high-entropy metal nitride including V, Cr, Nb, Mo, Zr	Mechanochemical-assisted urea glass route	Ag/AgCl	1 M KOH	230 F g^{-1} at 210 mV s^{-1}	n.a	n.a	−1 to 0 V	[157]
	3D Ni_3N nanosheet/CC [a]	Ammonolysis	Ag/AgCl	1 M KOH	990 F g^{-1} at 10 mA cm^{-2} 800 F g^{-1} at 40 mA cm^{-2}	2000	94%	−0.1 to 0.45 V	[166]
	VN nanoparticles	Ammonolysis	Hg/HgO	1 M KOH	554 F g^{-1} at 100 mV s^{-1}	1000	>90%	−1.2 – 0 V	[173]
	Nanostructured VN/CNTs composites [b]	Ammonolysis	Hg/HgO	6 M KOH	270 F g^{-1}	n.a	58% at 30 A g^{-1}	n.a	[172]
	core–shell (TiN-VN) fibers	Ammonolysis	SCE	1 M KOH	247.5 F g^{-1} at 2 mV s^{-1} 160.8 F g^{-1} at 50 mV s^{-1}	500	88%	−1.2 V to -0.2 V	[171]
	Self-supported carbon coated TiN nanotube arrays	Ammonolysis	Ag/AgCl	1 M KOH	167 F g^{-1} at 1.0 A g^{-1} 95 F g^{-1} at 50 A g^{-1}	6000	70%	−1 to 0V	[170]
	W_2N@carbon ultrathin layer core-shell structures	Ammonolysis	Ag/AgCl	2 M H_2SO_4	693 mF cm^{-2} at 5 mV s^{-1}	20,000	91%	−0.25 to 0.6 V	[169]
	Mo_3N_2 nanowires	Ammonolysis	Hg/HgO	1 M KOH	220 F g^{-1} at 50 mV s^{-1}	n.a	n.a	−1.1 to −0.3 V	[168]

[a] CC = Carbon cloth, [b] CNT = carbon nanotubes; n.a: represents that the corresponding data are not provided in the papers cited.

issues. Also, out-of-the-normal concept thinking and building up the exceptional nanostructures like defect-free 2D graphene might generate amazing outcomes. In addition, instead of demonstrating chemical/physical stability for few hours for electrocatalysis or few hundred cycles for LIBs/SIBs, maintaining high performance for orders of magnitude longer time/cycles is also of great importance.

As for electrocatalysis, bifunctionality of MTMPs and MTMNs as well as MTMBs towards HER and OER makes it stands out to be simplified anode/cathode to replace the IrO_2-Pt couple. However, future works are in needs to identify the real active sites of MTMPs, MTMNs, and MTMBs during the anodic half OER. Many open questions are still left open. For instance, if the surface hydroxides/oxyhydroxides in-situ generated under high oxidizing OER condition or the interface between phosphides nitrides/borides and hydroxides/oxyhydroxides the main contributor to high catalytic activity? Is the role of MTMPs and MTMNs only as conductive scaffold for the surface hydroxides/oxyhydroxides? To what extent the in-situ conversion process takes place; are the conversion the same for MTMPs, MTMNs, and MTMBs? In these regards, probing into atomic-level interfacial structure of catalysts during electrochemical reaction via in-situ spectroscopic surface analysis (Raman spectroscopy, XANES, EXAFS) would fit nicely. However, during electrocatalytic processes (i.e. HER, OER, and ORR), the drastic generation of hydrogen and oxygen make the measurements rather difficult. Therefore, advances in engineering characterization equipment is also necessary. Additionally, due to the importance of electrocatalyst surface, investigating and controlling surface-atoms arrangement and preferable exposed facets are of great interest to understand the mechanism behind. However, most of MLTMNs investigated so far are polycrystalline; synthesis methodology needs to be further accelerated. Equally important, theoretical calculations also need to be pushed forward to speculate the activity changes due to crystal structures, chemical states, doped-elements, interaction between materials in heterostructures. Answering these questions theoretically will help to have a comprehensive insight on how MLTMNs work and remain active during electrolysis; hence, speeding up the development of MLTMNs for energy conversion process. Another challenge is the surface oxidation of MTMPs, MTMNs, and MTMBs when stored at ambient conditions due to the under-coordinated non-metal sites. This may not affect OER performance but decrease the conductivity significantly and block HER active sites. In this respect, non-metal doping (S, Se-doping for examples) could be an effective way to suppress this issue. Although MTMPs and MTMNs show their superior performance in alkaline electrolyzer, IrO_2/RuO_2 is still the most active OER catalyst in acidic electrolyte. Hence, more efforts are needed to fulfill their full potential for energy conversion processes.

Compared to the above energy conversion process, the applications of MLTMNs in energy storage (batteries, supercapacitors) are less but increase rapidly due to the possibility of greatly enhanced properties. Despite the promising results initially, MLTMNs are still facing many obstacles on its way to commercialization. For examples, unsatisfied capacity, poor cycle stability resulting from volume changes/irreversible conversion reaction, lower conductivity/stability during electrode reactions; and most importantly, safety issues. To address these concerns, many post-engineering strategies to achieve plentiful pores and channels would partially help. Besides, reducing the content of inactive constituents (current collectors, binders) by developing self-support or binder-free electrode is promising. Moreover, extra efforts should be put by means of employing novel nanoscience and nanotechnologies to fabricate innovative materials and investigate their structural/composition optimization. An in-depth understanding of the mechanism by in-situ electrochemical and optical characterizations would be of great interest as well. Regarding applications toward supercapacitors, there is still a huge gap between the theoretical predicted specific capacitance and the one measured; while other performance indicators other than specific capacitance should be optimized as well. All things considered, researching and developing MLTMNs for energy storage and conversion is highly rewarding but daunting, in which slightly improvement might bring remarkable breakthroughs to the energy field.

Acknowledgements

The authors gratefully acknowledge the financial support from Singapore MOE AcRF Tier 1 under grant Nos. RG119/16 and 2017-T1-002-009, Singapore EMA project EIRP12/NRF2015EWT-EIRP002-008, and Guoxuan-NTU joint lab.

References

[1] V.C. Hoang, L.H. Nguyen, V.G. Gomes, J. Electroanal. Chem. 832 (2019) 87–96.
[2] I. Roger, M.A. Shipman, M.D. Symes, Nat. Rev. Chem. 1 (2017), 0003.
[3] K.N. Dinh, P. Zheng, Z. Dai, Y. Zhang, R. Dangol, Y. Zheng, B. Li, Y. Zong, Q. Yan, Small 14 (2018), 1703257.
[4] C.-F. Du, K.N. Dinh, Q. Liang, Y. Zheng, Y. Luo, J. Zhang, Q. Yan, Adv. Energy Mater. 8 (2018), 1801127.
[5] Z. Wang, X. Li, H. Ling, C.K. Tan, L.P. Yeo, A.C. Grimsdale, A.I.Y. Tok, Small 14 (2018), 1800395.
[6] G. Li, Y. Sun, J. Rao, J. Wu, A. Kumar, N. Xu Qiu, C. Fu, E. Liu, R. Blake Graeme, P. Werner, B. Shao, K. Liu, S. Parkin, X. Liu, M. Fahlman, S.-C. Liou, G. Auffermann, J. Zhang, C. Felser, X. Feng, Adv. Energy Mater. 0 (2018), 1801258.
[7] K.N. Dinh, P. Zheng, Z. Dai, Y. Zhang, R. Dangol, Y. Zheng, B. Li, Y. Zong, Q. Yan, Small 14 (2017), 1703257.
[8] P. Xiao, W. Chen, X. Wang, Adv. Energy Mater. 5 (2015), 1500985.
[9] S.T. Oyama, in: G. Ertl, H. Knözinger, F. Schüth, J. Weitkamp (Eds.), Handbook of Heterogeneous Catalysis: Online, 2008, pp. 342–356.
[10] H. Yu, K.N. Dinh, Y. Sun, H. Fan, Y. Wang, Y. Jing, S. Li, M. Srinivasan, Q. Yan, Nanoscale 10 (2018) 14877–14884.
[11] H. Li, X. Jia, Q. Zhang, X. Wang, Chem 4 (2018) 1510–1537.
[12] S. Carenco, D. Portehault, C. Boissière, N. Mézailles, C. Sanchez, Chem. Rev. 113 (2013) 7981–8065.
[13] B. Aronsson, Borides, Silicides and Phosphides, Methuen, London and Wiley, New York, 1965.
[14] G. Guo, Y. Guo, H. Tan, H. Yu, W. Chen, E. Fong, Q. Yan, J. Mater. Chem. A 4 (2016) 10893–10899.
[15] Z. Huang, Z. Chen, Z. Chen, C. Lv, H. Meng, C. Zhang, ACS Nano 8 (2014) 8121–8129.
[16] A.B. Laursen, K.R. Patraju, M.J. Whitaker, M. Retuerto, T. Sarkar, N. Yao, K.V. Ramanujachary, M. Greenblatt, G.C. Dismukes, Energy Environ. Sci. 8 (2015) 1027–1034.
[17] X. Chen, M. Cheng, D. Chen, R. Wang, ACS Appl. Mater. Interfaces 8 (2016) 3892–3900.
[18] J.F. Callejas, J.M. McEnaney, C.G. Read, J.C. Crompton, A.J. Biacchi, E.J. Popczun, T.R. Gordon, N.S. Lewis, R.E. Schaak, ACS Nano 8 (2014) 11101–11107.
[19] E.J. Popczun, J.R. McKone, C.G. Read, A.J. Biacchi, A.M. Wiltrout, N.S. Lewis, R.E. Schaak, J. Am. Chem. Soc. 135 (2013) 9267–9270.
[20] Y. Pan, Y. Liu, J. Zhao, K. Yang, J. Liang, D. Liu, W. Hu, D. Liu, Y. Liu, C. Liu, J. Mater. Chem. A 3 (2015) 1656–1665.
[21] J.F. Callejas, C.G. Read, E.J. Popczun, J.M. McEnaney, R.E. Schaak, Chem. Mater. 27 (2015) 3769–3774.
[22] D. Yang, J. Zhu, X. Rui, H. Tan, R. Cai, H.E. Hoster, D.Y.W. Yu, H.H. Hng, Q. Yan, ACS Appl. Mater. Interfaces 5 (2013) 1093–1099.
[23] J. Xu, Y. Zhao, C. Zou, Chem. Phys. Lett. 423 (2006) 138–142.
[24] E. Muthuswamy, P.R. Kharel, G. Lawes, S.L. Brock, ACS Nano 3 (2009) 2383–2393.
[25] S.C. Perera, G. Tsoi, L.E. Wenger, S.L. Brock, J. Am. Chem. Soc. 125 (2003) 13960–13961.
[26] R. Prins, M.E. Bussell, Catal. Lett. 142 (2012) 1413–1436.
[27] J. Liu, X. Chen, M. Shao, C. An, W. Yu, Y. Qian, J. Cryst. Growth 252 (2003) 297–301.
[28] Y. Ni, L. Jin, J. Hong, Nanoscale 3 (2011) 196–200.
[29] X. Wang, F. Wan, Y. Gao, J. Liu, K. Jiang, J. Cryst. Growth 310 (2008) 2569–2574.
[30] Y. Xie, H.L. Su, X.F. Qian, X.M. Liu, Y.T. Qian, J. Solid State Chem. 149 (2000) 88–91.
[31] S. Liu, Y. Qian, X. Ma, Mater. Lett. 62 (2008) 11–14.
[32] Y. Ni, J. Li, L. Zhang, S. Yang, X. Wei, Mater. Res. Bull. 44 (2009) 1166–1172.
[33] F. Luo, H.-L. Su, W. Song, Z.-M. Wang, Z.-G. Yan, C.-H. Yan, J. Mater. Chem. 14 (2004) 111–115.
[34] S. Liu, X. Liu, L. Xu, Y. Qian, X. Ma, J. Cryst. Growth 304 (2007) 430–434.

[35] Y.H. Budnikova, D.I. Tazeev, B.A. Trofimov, O.G. Sinyashin, Electrochem. Commun. 6 (2004) 700–702.
[36] L. Zhong-Zhen, Z. Yu, Z. Chaohua, T.H. Teng, L. Zhong, A. Anas, W. Xing-Long, X. Qihua, K.K. Aik, H. Kedar, X. Jianwei, H.H. Hoon, Y. Qingyu,Adv. Energy Mater. 7 (2017), 1601285.
[37] Y. Lin, Y. Pan, J. Zhang, Int. J. Hydrog. Energy 42 (2017) 7951–7956.
[38] J. Wang, D. Liu, H. Huang, N. Yang, B. Yu, M. Wen, X. Wang, P.K. Chu, X.-F. Yu, Angew. Chem. 130 (2017) 2630–2634.
[39] K.Y. Yoon, Y. Jang, J. Park, Y. Hwang, B. Koo, J.-G. Park, T. Hyeon, J. Solid State Chem. 181 (2008) 1609–1613.
[40] H. Liang, A.N. Gandi, D.H. Anjum, X. Wang, U. Schwingenschlögl, H.N. Alshareef, Nano Lett. 16 (2016) 7718–7725.
[41] B. Qiu, L. Cai, Y. Wang, Z. Lin, Y. Zuo, M. Wang, Y. Chai, Adv. Funct. Mater. 28 (2018), 1706008.
[42] B. Zhang, Y.H. Lui, H. Ni, S. Hu, Nano Energy 38 (2017) 553–560.
[43] M. Qian, S. Cui, D. Jiang, L. Zhang, P. Du, Adv. Mater. 29 (2017), 1704075.
[44] X.-D. Wang, H.-Y. Chen, Y.-F. Xu, J.-F. Liao, B.-X. Chen, H.-S. Rao, D.-B. Kuang, C.-Y. Su, J. Mater. Chem. A 5 (2017) 7191–7199.
[45] P. He, X.-Y. Yu, W. Lou Xiong, Angew. Chem. Int. Ed. 56 (2017) 3897–3900.
[46] L. Yu, I.K. Mishra, Y. Xie, H. Zhou, J. Sun, J. Zhou, Y. Ni, D. Luo, F. Yu, Y. Yu, S. Chen, Z. Ren, Nano Energy 53 (2018) 492–500.
[47] Y. Feng, H. Zhang, Y. Mu, W. Li, J. Sun, K. Wu, Y. Wang, Chem. Eur. J. 21 (2015) 9229–9235.
[48] Z. Liang, R. Huo, S. Yin, F. Zhang, S. Xu, J. Mater. Chem. A 2 (2014) 921–925.
[49] Y. Bai, H. Zhang, L. Fang, L. Liu, H. Qiu, Y. Wang, J. Mater. Chem. A 3 (2015) 5434–5441.
[50] W.-J. Li, Q.-R. Yang, S.-L. Chou, J.-Z. Wang, H.-K. Liu, J. Power Sources 294 (2015) 627–632.
[51] J. Liu, P. Kopold, C. Wu, P.A. van Aken, J. Maier, Y. Yu, Energy Environ. Sci. 8 (2015) 3531–3538.
[52] Y. Zhang, H. Zhang, Y. Feng, L. Liu, Y. Wang, ACS Appl. Mater. Interfaces 7 (2015) 26684–26690.
[53] X. Wang, P. Sun, J. Qin, J. Wang, Y. Xiao, M. Cao, Nanoscale 8 (2016) 10330–10338.
[54] Y. Bai, H. Zhang, L. Liu, H. Xu, Y. Wang, Chem. Eur. J. 22 (2015) 1021–1029.
[55] H. Zhang, Y. Feng, Y. Zhang, L. Fang, W. Li, Q. Liu, K. Wu, Y. Wang, ChemSusChem 7 (2014) 2000–2006.
[56] C. An, Y. Wang, L. Li, F. Qiu, Y. Xu, C. Xu, Y. Huang, L.J.H. Yuan, Electrochim. Acta 133 (2014) 180–187.
[57] Y.-M. Hu, M.-C. Liu, Y.-X. Hu, Q.-Q. Yang, L.-B. Kong, L. Kang, Electrochim. Acta 215 (2016) 114–125.
[58] H. Wan, L. Li, Y. Chen, J. Gong, M. Duan, C. Liu, J. Zhang, H. Wang, Electrochim. Acta 229 (2017) 380–386.
[59] C. An, Y. Wang, Y. Wang, G. Liu, L. Li, F. Qiu, Y. Xu, L. Jiao, H. Yuan, RSC Adv. 3 (2013) 4628–4633.
[60] Y. Lu, J.-k. Liu, X.-y. Liu, S. Huang, T.-q. Wang, X.-l. Wang, C.-d. Gu, J.-p. Tu, S.X. Mao, CrystEngComm 15 (2013) 7071–7079.
[61] K. Zhou, W. Zhou, L. Yang, J. Lu, S. Cheng, W. Mai, Z. Tang, L. Li, S. Chen, Adv, Funct. Mater. 25 (2015) 7530–7538.
[62] P. Liu, J.A. Rodriguez, J. Am. Chem. Soc. 127 (2005) 14871–14878.
[63] K. Xu, H. Cheng, H. Lv, J. Wang, L. Liu, S. Liu, X. Wu, W. Chu, C. Wu, Y. Xie, Adv. Mater. 30 (2017), 1703322.
[64] B. Liu, H. Li, B. Cao, J. Jiang, R. Gao, J. Zhang, Adv. Funct. Mater. 0 (2018), 1801527.
[65] M. Hou, X. Teng, J. Wang, Y. Liu, L. Guo, L. Ji, C. Cheng, Z. Chen, Nanoscale (2018).
[66] Z. Pu, Q. Liu, A.M. Asiri, X. Sun, ACS Appl. Mater. Interfaces 6 (2014) 21874–21879.
[67] J. Hao, W. Yang, Z. Huang, C. Zhang, Adv. Mater. Interfaces 3 (2016), 1600236.
[68] L. Yunxiang, Y. Li, Z. Youkui, J. Hongliang, X. Zijian, W. Chuanqiang, Z. Guobin, J. Jun, S. Li, Adv. Energy Mater. 8 (2018), 1703623.
[69] B. Weng, C.R. Grice, W. Meng, L. Guan, F. Xu, Y. Yu, C. Wang, D. Zhao, Y. Yan, ACS Energy Lett. 3 (2018) 1434–1442.
[70] T. Meng, Y.-N. Hao, L. Zheng, M. Cao, Nanoscale (2018).
[71] Y. Liang, Q. Liu, A.M. Asiri, X. Sun, Y. Luo, ACS Catal. 4 (2014) 4065–4069.
[72] X. Wang, W. Li, D. Xiong, D.Y. Petrovykh, L. Liu, Adv. Funct. Mater. 26 (2016) 4067–4077.
[73] J. Tian, Q. Liu, A.M. Asiri, X. Sun, J. Am. Chem. Soc. 136 (2014) 7587–7590.
[74] Y. Shi, Y. Xu, S. Zhuo, J. Zhang, B. Zhang, ACS Appl. Mater. Interfaces 7 (2015) 2376–2384.
[75] J. Deng, P. Ren, D. Deng, X. Bao, Angew. Chem. Int. Ed. 54 (2015) 2100–2104.
[76] Q. Liu, J. Tian, W. Cui, P. Jiang, N. Cheng, A.M. Asiri, X. Sun, Angew. Chem. Int. Ed. 53 (2014) 6710–6714.
[77] C. Ray, S.C. Lee, B. Jin, A. Kundu, J.H. Park, S.C. Jun, ACS Sustain, Chem. Eng. 6 (2018) 6146–6156.
[78] K.N. Dinh, X. Sun, Z. Dai, Y. Zheng, P. Zheng, J. Yang, J. Xu, Z. Wang, Q. Yan, Nano Energy 54 (2018) 82–90.
[79] K. Chen, X. Huang, C. Wan, H. Liu, RSC Adv. 5 (2015) 92893–92898.
[80] V.V.T. Doan-Nguyen, S. Zhang, E.B. Trigg, R. Agarwal, J. Li, D. Su, K.I. Winey, C.B. Murray, ACS Nano 9 (2015) 8108–8115.
[81] C. Han, X. Bo, Y. Zhang, M. Li, A. Wang, L. Guo, Chem. Commun. 51 (2015) 15015–15018.
[82] H.H. Hwu, J.G. Chen, Chem. Rev. 105 (2005) 185–212.
[83] K. Huang, Z. Li, J. Lin, G. Han, P. Huang, Chem. Soc. Rev. 47 (2018) 5109–5124.
[84] M. Alhabeb, K. Maleski, B. Anasori, P. Lelyukh, L. Clark, S. Sin, Y. Gogotsi, Chem. Mater. 29 (2017) 7633–7644.
[85] B. Anasori, M.R. Lukatskaya, Y. Gogotsi, Nat. Rev. Materials 2 (2017) 16098.
[86] X. Tao, J. Du, Y. Li, Y. Yang, Z. Fan, Y. Gan, H. Huang, W. Zhang, L. Dong, X. Li, V, ter. 1 (2011) 534–539.
[87] Y.-J. Tang, C.-H. Liu, W. Huang, X.-L. Wang, L.-Z. Dong, S.-L. Li, Y.-Q. Lan, ACS Appl. Mater. Interfaces 9 (2017) 16977–16985.
[88] Q. Liang, L. Ye, Z.-H. Huang, Q. Xu, Y. Bai, F. Kang, Q.-H. Yang, Nanoscale 6 (2014) 13831–13837.
[89] Z. Kou, T. Meng, B. Guo, I.S. Amiinu, W. Li, J. Zhang, S. Mu, Adv. Funct. Mater. 27 (2017), 1604904.
[90] S.K. Kim, Y. Qiu, Y.-J. Zhang, R. Hurt, A. Peterson, Appl. Catal. B-Environ. 235 (2018) 36–44.
[91] J. Gautam, T.D. Thanh, K. Maiti, N.H. Kim, J.H. Lee, Carbon 137 (2018) 358–367.
[92] H. Wang, Y. Zhang, H. Ang, Y. Zhang, H.T. Tan, Y. Zhang, Y. Guo, J.B. Franklin, X.L. Wu, M. Srinivasan, H.J. Fan, Q. Yan, Adv. Funct. Mater. 26 (2016) 3082–3093.
[93] C. Xu, L. Wang, Z. Liu, L. Chen, J. Guo, N. Kang, X.-L. Ma, H.-M. Cheng, W. Ren, Nat. Mater. (2015) 14.
[94] M. Zeng, Y. Chen, J. Li, H. Xue, R.G. Mendes, J. Liu, T. Zhang, M.H. Rümmeli, L. Fu, Nano Energy 33 (2017) 356–362.
[95] V.G. Harris, Y. Chen, A. Yang, S. Yoon, Z. Chen, A.L. Geiler, J. Gao, C.N. Chinnasamy, L.H. Lewis, C. Vittoria, E.E. Carpenter, K.J. Carroll, R. Goswami, M.A. Willard, L. Kurihara, M. Gjoka, O. Kalogirou, Journal of Physics D: Appl. Phys. 43 (2010), 165003.
[96] Z. Chen, L. Liu, Q. Chen, Mater. Lett. 164 (2016) 554–557.
[97] D.V. Esposito, S.T. Hunt, Y.C. Kimmel, J.G. Chen, J. Am. Chem. Soc. 134 (2012) 3025–3033.
[98] N. Lyakhov, T. Grigoreva, V. Šepelák, B. Tolochko, A. Ancharov, S. Vosmerikov, E. Devyatkina, T. Udalova, S. Petrova, J. Mater. Science 53 (2018) 13584–13591.
[99] W. Hao-Fan, T. Cheng, W. Bin, L. Bo-Quan, Z. Qiang, Adv. Mater. 29 (2017), 1702327.
[100] L. Cao, N. Zhang, L. Feng, J. Huang, Y. Feng, W. Li, D. Yang, Q. Liu, Nanoscale (2018).
[101] H. Ang, H.T. Tan, Z.M. Luo, Y. Zhang, Y.Y. Guo, G. Guo, H. Zhang, Q. Yan, Small 11 (2015) 6278–6284.
[102] H.B. Wu, B.Y. Xia, L. Yu, X.-Y. Yu, X.W. Lou, Nat. Commun. 6 (2015) 6512.
[103] H. Ang, H. Wang, B. Li, Y. Zong, X. Wang, Q. Yan, Small 12 (2016) 2859–2865.
[104] X. Sang, Y. Xie, D.E. Yilmaz, R. Lotfi, M. Alhabeb, A. Ostadhossein, B. Anasori, W. Sun, X. Li, K. Xiao, P.R.C. Kent, A.C.T. van Duin, Y. Gogotsi, R.R. Unocic, Nat. Commun. 9 (2018) 2266.
[105] Y. Xiao, J.-Y. Hwang, Y.-K. Sun, J. Mater. Chem. A 4 (2016) 10379–10393.
[106] Y. Zhong, X. Xia, F. Shi, J. Zhan, J. Tu, H.J. Fan, Adv. Sci. 3 (2016), 1500286.
[107] H. Zhang, Z. Fu, R. Zhang, Q. Zhang, H. Tian, D. Legut, T.C. Germann, Y. Guo, S. Du, J.S. Francisco, Proc. Natl. Acad. Sci. 114 (2017) E11082–E11091.
[108] M.-Q. Zhao, M. Torelli, C.E. Ren, M. Ghidiu, Z. Ling, B. Anasori, M.W. Barsoum, Y. Gogotsi, Nano Energy 30 (2016) 603–613.
[109] W. Yang, S. Rehman, X. Chu, Y. Hou, S. Gao, ChemNanoMat 1 (2015) 376–398.
[110] Y.-T. Weng, N.-L. Wu, Chem. Commun. 49 (2013) 10784–10786.
[111] J. Zhu, K. Sakaushi, G. Clavel, M. Shalom, M. Antonietti, T.-P. Fellinger, J. Am. Chem. Soc. 137 (2015) 5480–5485.
[112] S. Liu, F. Li, D. Wang, C. Huang, Y. Zhao, J.B. Baek, J. Xu,Small Methods (2018), 1800040.
[113] T. Yu, S. Zhang, F. Li, Z. Zhao, L. Liu, H. Xu, G. Yang, J. Mater. Chem. A 5 (2017) 18698–18706.
[114] J. Liu, S. Tang, Y. Lu, G. Cai, S. Liang, W. Wang, X. Chen, Energy Environ. Sci. 6 (2013) 2691–2697.
[115] M. Deng, J. Qi, X. Li, Y. Xiao, L. Yang, X. Yu, H. Wang, B. Yuan, Q. Gao, Electrochim. Acta 277 (2018) 205–210.
[116] X. Li, M. Deng, W. Zhang, Q. Gao, H. Wang, B. Yuan, L. Yang, M. Zhu, Mater. Lett. 194 (2017) 30–33.
[117] E. Yang, H. Ji, J. Kim, H. Kim, Y. Jung, Phys. Chem. Chem. Phys. 17 (2015) 5000–5005.
[118] T. Yu, Z. Zhao, L. Liu, S. Zhang, H. Xu, G. Yang, J. Am. Chem. Soc. 140 (2018) 5962–5968.
[119] M. Li, S. Yu, Z. Chen, Z. Wang, F. Lv, B. Nan, Y. Zhu, Y. Shi, W. Wang, S. Wu, H. Liu, Y. Tang, Z. Lu, Inorg. Chem. Front. 4 (2017) 289–295.
[120] X. Xia, Y. Zhang, D. Chao, Q. Xiong, Z. Fan, X. Tong, J. Tu, H. Zhang, H.J. Fan, Energy Environ. Sci. 8 (2015) 1559–1568.
[121] T. Yu, S. Zhang, F. Li, Z. Zhao, L. Liu, H. Xu, G. Yang, J. Mater. Chem. A 5 (2017) 18698–18706.
[122] H. Wan, Y. Liu, H. Zhang, W. Zhang, N. Jiang, Z. Wang, S. Luo, H. Arandiyan, H. Liu, H. Sun, Electrochim. Acta 281 (2018) 31–38.
[123] H. Zhang, J. Liu, Z. Tian, Y. Ye, Y. Cai, C. Liang, K. Terabe, Carbon 100 (2016) 590–599.
[124] T. Morishita, Y. Soneda, H. Hatori, M. Inagaki, Electrochim. Acta 52 (2007) 2478–2484.
[125] L.H. Bennett, J.R. Cuthill, A.J. McAlister, N.E. Erickson, R.E. Watson, Science 184 (1974) 563–565.
[126] Q. Gong, Y. Wang, Q. Hu, J. Zhou, R. Feng, P.N. Duchesne, P. Zhang, F. Chen, N. Han, Y. Li, C. Jin, Y. Li, S.-T. Lee, Nat. Commun. 7 (2016) 13216.
[127] S. Emin, C. Altinkaya, A. Semerci, H. Okuyucu, A. Yildiz, P. Stefanov, Appl. Catal. B-Environ. 236 (2018) 147–153.
[128] S. Li, C. Yang, Z. Yin, H. Yang, Y. Chen, L. Lin, M. Li, W. Li, G. Hu, D. Ma, Nano Res. 10 (2017) 1322–1328.
[129] H. Chunyong, T. Juzhou, Chem. Commun. 51 (2015) 8323–8325.

[130] L. Zhang, H. Yang, D.K.J.A. Wanigarathna, B. Liu,Small Methods 2 (2018), 1700353.
[131] J. Jiang, Q. Liu, C. Zeng, L. Ai, J. Mater. Chem. A 5 (2017) 16929–16935.
[132] H. Wang, Y. Cao, C. Sun, G. Zou, J. Huang, X. Kuai, J. Zhao, L. Gao, ChemSusChem 10 (2017) 3540–3546.
[133] D. Das, S. Santra, K.K. Nanda, ACS Appl. Mater. Interfaces 10 (2018) 35025–35038.
[134] J. Su, G. Xia, R. Li, Y. Yang, J. Chen, R. Shi, P. Jiang, Q. Chen, J. Mater. Chem. A 4 (2016) 9204–9212.
[135] T. Huang, J. Yu, J. Han, Z. Zhang, Y. Xing, C. Wen, X. Wu, Y. Zhang, J. Power Sources 300 (2015) 483–490.
[136] Y.C. Kimmel, X. Xu, W. Yu, X. Yang, J.G. Chen, ACS Catal. 4 (2014) 1558–1562.
[137] J. Guo, Z. Mao, X. Yan, R. Su, P. Guan, B. Xu, X. Zhang, G. Qin, S.J. Pennycook, Nano Energy 28 (2016) 261–268.
[138] H. Fan, H. Yu, Y. Zhang, Y. Zheng, Y. Luo, Z. Dai, B. Li, Y. Zong, Q. Yan, Angew. Chem. Int. Ed. 56 (2017) 12566–12570.
[139] X. Ma, H. Meng, M. Cai, P.K. Shen, J. Am. Chem. Soc. 134 (2012) 1954–1957.
[140] C. He, J. Tao, J. Catal. 347 (2017) 63–71.
[141] N.N. Greenwood, A. Earnshaw, Chemistry of the Elements, 2nd ed., Butterworth-Heinemann, Oxford, 1997.
[142] R.B. Anderson, in: W.G. Frankenburg, V.I. Komarewsky, E.K. Rideal (Eds.), Advances in Catalysis, Academic Press, 1953, pp. 355–384.
[143] L. Imhoff, A. Bouteville, J.C. Remy, J. Electrochem. Soc. 145 (1998) 1672–1677.
[144] M. Ritala, M. Leskelä, E. Rauhala, J. Jokinen, J. Electrochem. Soc. 145 (1998) 2914–2920.
[145] D. Rische, H. Parala, E. Gemel, M. Winter, R.A. Fischer, Chem. Mater. 18 (2006) 6075–6082.
[146] C. Zhu, P. Yang, D. Chao, X. Wang, X. Zhang, S. Chen, B.K. Tay, H. Huang, H. Zhang, W. Mai, H.J. Fan, Adv. Mater. 27 (2015) 4566–4571.
[147] Y. Zhang, B. Ouyang, J. Xu, S. Chen, R.S. Rawat, H.J. Fan, Adv. Energy Mater. 6 (2016), 1600221.
[148] C. Zhu, Y. Sun, D. Chao, X. Wang, P. Yang, X. Zhang, H. Huang, H. Zhang, H.J. Fan, Nano Energy 26 (2016) 1–6.
[149] W. Kim, J.S. Park, C.Y. Suh, S.W. Cho, S. Lee, I.J. Shon, Mater. Trans. 50 (2009) 2897–2899.
[150] I. Grzegory, J. Jun, M. Boćkowski, S.T. Krukowski, M. Wróblewski, B. Łucznik, S. Porowski, J. Phys. Chem. Solids 56 (1995) 639–647.
[151] J. Schmitt, Google Patents, 2013.
[152] Y. Zhang, R.S. Rawat, H.J. Fan, Small Methods 1 (2017), 1700164.
[153] S. Han, X. Hu, J. Wang, X. Fang, Y. Zhu, Adv. Energy Mater. 8 (2018), 1800955.
[154] X. He, Y. Shuai, L. Na, K. Chen, Y. Zhang, Z. Zhang, F. Gan, Mater. Lett. 215 (2018) 91–94.
[155] C. Giordano, C. Erpen, W. Yao, M. Antonietti, Nano Lett. 8 (2008) 4659–4663.
[156] C. Giordano, C. Erpen, W. Yao, B. Milke, M. Antonietti, Chem. Mater. 21 (2009) 5136–5144.
[157] T. Jin, X. Sang, R.R. Unocic, R.T. Kinch, X. Liu, J. Hu, H. Liu, S. Dai, Adv. Mater. (2018) 30.
[158] X. Lu, G. Wang, T. Zhai, M. Yu, S. Xie, Y. Ling, C. Liang, Y. Tong, Y. Li, Nano Lett. 12 (2012) 5376–5381.
[159] S. Wang, X. Yu, Z. Lin, R. Zhang, D. He, J. Qin, J. Zhu, J. Han, L. Wang, H.-k. Mao, J. Zhang, Y. Zhao, Chem. Mater. 24 (2012) 3023–3028.
[160] M.-S. Balogun, M. Yu, C. Li, T. Zhai, Y. Liu, X. Lu, Y. Tong, J. Mater. Chem. A 2 (2014) 10825–10829.
[161] H. Zhou, Z. Li, K. Wang, M. Gao, S. Ding, J. Mater. Chem. A (2019).
[162] M. Zhang, Y. Qiu, Y. Han, Y. Guo, F. Cheng, J. Power Sources 322 (2016) 163–168.
[163] M.-S. Balogun, M. Yu, Y. Huang, C. Li, P. Fang, Y. Liu, X. Lu, Y. Tong, Nano Energy 11 (2015) 348–355.
[164] Y. Dong, B. Wang, K. Zhao, Y. Yu, X. Wang, L. Mai, S. Jin, Nano Lett. 17 (2017) 5740–5746.
[165] L. Wang, J. Sun, R. Song, S. Yang, H. Song, Adv. Energy Mater. 6 (2016), 1502067.
[166] M.-S. Balogun, Y. Zeng, W. Qiu, Y. Luo, A. Onasanya, T.K. Olaniyi, Y. Tong, J. Mater. Chem. A 4 (2016) 9844–9849.
[167] B. Ouyang, Y. Zhang, Z. Zhang, H.J. Fan, R.S. Rawat, Small (2017) 13.
[168] K.-H. Lee, Y.-W. Lee, A.R. Ko, G. Cao, K.-W. Park, J. Am. Ceram. Soc. 96 (2013) 37–39.
[169] G. He, M. Ling, X. Han, D.I. Abou El Amaiem, Y. Shao, Y. Li, W. Li, S. Ji, B. Li, Y. Lu, R. Zou, F. Ryan Wang, D.J.L. Brett, Z. Xiao Guo, C. Blackman, I.P. Parkin, Energy Storage Mater. 9 (2017) 119–125.
[170] F. Grote, H. Zhao, Y. Lei, J. Mater. Chem. A 3 (2015) 3465–3470.
[171] X. Zhou, C. Shang, L. Gu, S. Dong, X. Chen, P. Han, L. Li, J. Yao, Z. Liu, H. Xu, Y. Zhu, G. Cui, ACS Appl. Mater. Interfaces 3 (2011) 3058–3063.
[172] C.M. Ghimbeu, E. Raymundo-Piñero, P. Fioux, F. Béguin, C. Vix-Guterl, J. Mater. Chem. 21 (2011) 13268–13275.
[173] D. Choi, G.E. Blomgren, P.N. Kumta, Adv. Mater. 18 (2006) 1178–1182.
[174] J.G. Chen, Chem. Rev. 96 (1996) 1477–1498.
[175] M. Jiang, Y. Li, Z. Lu, X. Sun, X. Duan, Inorg. Chem. Front. 3 (2016) 630–634.
[176] Y. Wang, D. Liu, Z. Liu, C. Xie, J. Huo, S. Wang, Chem. Commun. 52 (2016) 12614–12617.
[177] Y. Zhang, B. Ouyang, J. Xu, G. Jia, S. Chen, R.S. Rawat, H.J. Fan, Angew. Chem. Int. Ed. 55 (2016) 8670–8674.
[178] Z. Yin, Y. Sun, C. Zhu, C. Li, X. Zhang, Y. Chen, J. Mater. Chem. A 5 (2017) 13648–13658.
[179] F. Yu, H. Zhou, Z. Zhu, J. Sun, R. He, J. Bao, S. Chen, Z. Ren, ACS Catal. 7 (2017) 2052–2057.
[180] C. Walter, P.W. Menezes, S. Orthmann, J. Schuch, P. Connor, B. Kaiser, M. Lerch, M. Driess, Angew. Chem. 130 (2018) 706–710.
[181] V.R.B. Gurram, S.S. Enumula, R.R. Chada, K.S. Koppadi, D.R. Burri, S.R.R. Kamaraju, Catal. Surv. Asia 22 (2018) 166–180.
[182] Y. Zhong, X. Xia, F. Shi, J. Zhan, J. Tu, H.J. Fan, Adv. Sci. 3 (2016), 1500286.
[183] S.H. Gage, B.G. Trewyn, C.V. Ciobanu, S. Pylypenko, R.M. Richards, Catal. Sci. Technol. 6 (2016) 4059–4076.
[184] A.M. Alexander, J.S. Hargreaves, Chem. Soc. Rev. 39 (2010) 4388–4401.
[185] Y. Zhu, G. Chen, Y. Zhong, W. Zhou, Z. Shao, Adv. Sci. 5 (2018).
[186] Z. Chen, Y. Ha, Y. Liu, H. Wang, H. Yang, H. Xu, Y. Li, R. Wu, ACS Appl. Mater. Interfaces 10 (2018) 7134–7144.
[187] Q. Liang, L. Zhong, C. Du, Y. Luo, Y. Zheng, S. Li, Q. Yan, Nano Energy 47 (2018) 257–265.
[188] B. Konkena, J. Masa, A.J.R. Botz, I. Sinev, W. Xia, J. Kossmann, R. Drautz, M. Muhler, W. Schuhmann, ACS Catal. 7 (2017) 229–237.
[189] M. Kuang, Q. Wang, H. Ge, P. Han, Z. Gu, A.M. Al-Enizi, G. Zheng, ACS Energy Lett. 2 (2017) 2498–2505.
[190] Y. Shi, B. Zhang, Chem. Soc. Rev. 45 (2016) 1529–1541.
[191] M. Gong, H. Dai, Nano Res. 8 (2015) 23–39.
[192] S. Nandi, S.K. Singh, D. Mullangi, R. Illathvalappil, L. George, C.P. Vinod, S. Kurungot, R. Vaidhyanathan,Adv. Energy Mater. 6 (2016), 1601189.
[193] H. Abroshan, P. Bothra, S. Back, A. Kulkarni, J.K. Norskov, S. Siahrostami, J. Phys. Chem. C 122 (2018) 4783–4791.
[194] H. Tang, J. Luo, J. Yu, W. Zhao, H. Song, S. Liao, Chemelectrochem 5 (2018) 2041–2049.
[195] U.B. Demirci, P. Miele, Phys. Chem. Chem. Phys. 12 (2010) 14651–14665.
[196] J.M.V. Nsanzimana, Y. Peng, Y.Y. Xu, L. Thia, C. Wang, B.Y. Xia, X. Wang, Adv. Energy Mater. 8 (2017), 1701475.
[197] L. Xu, S. Li, Y. Zhang, Y. Zhai, Nanoscale 4 (2012) 4900–4915.
[198] X. Wang, G. Tai, Z. Wu, T. Hu, R. Wang, J. Mater. Chem. A 5 (2017) 23471–23475.
[199] L. Chen, Y. Gu, L. Shi, Z. Yang, J. Ma, Y. Qian, J. Alloys. Compd. 368 (2004) 353–356.
[200] H. Park, A. Encinas, J.P. Scheifers, Y. Zhang, B.P.T. Fokwa, Angew. Chem. Int. Ed. 56 (2017) 5575–5578.
[201] H.O. Pierson, E. Randich, Thin Solid Films 54 (1978) 119–128.
[202] T. Takahashi, H. Kamiya, J. Cryst. Growth 26 (1974) 203–209.
[203] T.M. Besmann, K.E. Spear, J. Cryst. Growth 31 (1975) 60–65.
[204] Q. Ding, Y. Zhao, J. Xu, C. Zou, Solid State Commun. 141 (2007) 53–56.
[205] Q.Y. Zhang, J.Q. Xu, Y.M. Zhao, X.H. Ji, S.P. Lau, Adv. Funct. Mater. 19 (2009) 742–747.
[206] J.R. Brewer, R.M. Jacobberger, D.R. Diercks, C.L. Cheung, Chem. Mater. 23 (2011) 2606–2610.
[207] R. Wagner, W. Ellis, Appl. Phys. Lett. 4 (1964) 89–90.
[208] W.-J. Jiang, S. Niu, T. Tang, Q.-H. Zhang, X.-Z. Liu, Y. Zhang, Y.-Y. Chen, J.-H. Li, L. Gu, L.-J. Wan, J.-S. Hu, Angew. Chem. Int. Ed. 56 (2017) 6572–6577.
[209] J. Masa, I. Sinev, H. Mistry, E. Ventosa, M. de la Mata, J. Arbiol, M. Muhler, B. Roldan Cuenya, W. Schuhmann,Adv. Energy Mater. 7 (2017), 1700381.
[210] S. Klemenz, J. Schuch, S. Hawel, A.-M. Zieschang, B. Kaiser, W. Jaegermann, B. Albert, ChemSusChem 11 (2018) 3150–3156.
[211] Y. Wang, L. Li, Y. Wang, D. Song, G. Liu, Y. Han, L. Jiao, H. Yuan, J. Power Sources 196 (2011) 5731–5736.
[212] C. Wu, Y. Bai, F. Wu, X. Wang, J.-y. Lu, C. Qiao, Electrochem. Commun. 11 (2009) 2173–2176.
[213] C. Wu, Y. Bai, X. Wang, F. Wu, C.-z. Zhang, Solid State Ion. 179 (2008) 924–927.
[214] Y. Bai, C. Wu, F. Wu, L.-x. Yang, B.-r. Wu, Electrochem. Commun 11 (2009) 145–148.
[215] Z. Guo, J. Zhou, Z. Sun, J. Mater. Chem. A 5 (2017) 23530–23535.
[216] I.-s. Kim, G.E. Blomgren, P.N. Kumta, Electrochem. Solid-State Lett. 6 (2003) A157–A161.
[217] H. Vrubel, X. Hu, Angew. Chem. 124 (2012) 12875–12878.
[218] M. Zeng, H. Wang, C. Zhao, J. Wei, K. Qi, W. Wang, X. Bai, ChemCatChem 8 (2016) 708–712.
[219] H. Park, A. Encinas, J.P. Scheifers, Y. Zhang, B.P. Fokwa, Angew. Chem. Int. Ed. 56 (2017) 5575–5578.
[220] M. Sheng, Q. Wu, Y. Wang, F. Liao, Q. Zhou, J. Hou, W. Weng, Electrochem. Commun. 93 (2018) 104–108.
[221] N. Xu, G. Cao, Z. Chen, Q. Kang, H. Dai, P. Wang, J. Mater. Chem. A 5 (2017) 12379–12384.
[222] P. Zhang, M. Wang, Y. Yang, T. Yao, H. Han, L. Sun, Nano Energy 19 (2016) 98–107.
[223] T. Osaka, H. Ishibashi, T. Endo, T. Yoshida, Electrochim. Acta 26 (1981) 339–343.
[224] W.J. Jiang, S. Niu, T. Tang, Q.H. Zhang, X.Z. Liu, Y. Zhang, Y.Y. Chen, J.H. Li, L. Gu, L.J. Wan, Angew. Chem. 129 (2017) 6672–6677.
[225] J. Zhang, X. Li, Y. Liu, Z. Zeng, X. Cheng, Y. Wang, W. Tu, M. Pan, Nanoscale 10 (2018) 11997–12002.
[226] K. Elumeeva, J. Masa, D. Medina, E. Ventosa, S. Seisel, Y.U. Kayran, A. Genç, T. Bobrowski, P. Weide, J. Arbiol, J. Mater. Chem. A 5 (2017) 21122–21129.

Khang Ngoc Dinh received his B.S. degree in Chemistry from VNU University of Science, Vietnam in 2015. Currently, he is a Ph.D. candidate at the Interdisciplinary Graduate School of Nanyang Technological University in Singapore under the supervision of Prof. Qingyu Yan. His current research interests are on two main area: (1) synthesis and engineer of novel two-dimensional material for energy storage and conversion; (2) catalytic devices fabrication for electrocatalysis enhancement.

Qinghua Liang is currently a postdoctoral research fellow at Nanyang Technological University, Singapore. He received his B.S. and M.S. from Southwest University and Technical Institute of Physics and Chemistry of Chinese Academy of Sciences in 2009 and 2012, respectively. Then he received Ph.D. in Materials Science and Engineering from Tsinghua University in 2016. His research interests are the design and preparation of functional materials for energy storage and conversion.

Chengfeng Du is currently a postdoctoral research fellow at Nanyang Technological University in Singapore. He obtained his BS degree from Ocean University, China, in 2011 and Ph.D. degree from the Fujian Institute of Research on the Structure of Matter, Chinese Academy of Sciences, in 2016 under the supervision of Prof. Xiao-Ying Huang. His research interests focus on the synthesis and assembly of 2D-based hybrid materials and their applications to energy conversion and storage.

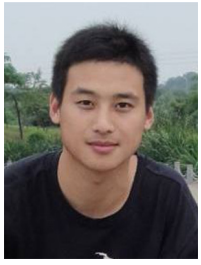

Jin Zhao Jin Zhao received his Ph.D. degree in chemistry from Nanjing University in 2016. He is currently a postdoctoral research fellow at Department of Materials Science & Engineering, Nanyang Technological University, Singapore. His current research interests focus on energy storage and electrocatalysis.

Alfred Iing Yoong Tok has been a faculty member in the School of Materials Science and Engineering, Nanyang Technological University since 2003. He obtained his Ph.D. in 2000 at Nanyang Technological University. In 2009, he was appointed Division Head of Materials Technology in MSE (till 2012). Since 2011, he has been the Deputy Director of the Institute for Sports Research in NTU. His research areas focus on the processing and applications of inorganic materials in the areas of biosensors and renewable/sustainable energy.

Hui Mao is currently an associate professor in College of Chemistry and Materials Science in Sichuan Normal University. She obtained her Ph.D. from Biomass Chemistry and Engineering Department of Sichuan University. She joined School of Materials Science and Engineering of Nanyang Technological University as a postdoctoral research fellow. She then joined College of Chemistry and Materials Science of Sichuan Normal University as an assistant professor in 2012 and became an associate professor in 2015. Mao's research focus on advanced electrode materials based on biomass and functional materials for the treatment of environmental pollutants.

Qingyu Yan is currently a professor in School of Materials Science and Engineering in Nanyang Technology University. He obtained his B.S. in Materials Science and Engineering, Nanjing University. He finished his Ph.D. from Materials Science and Engineering Department of State University of New York at Stony Brook. After that, he joined the Materials Science and Engineering Department of Rensselaer Polytechnic Institute as a postdoctoral research associate. He joined School of Materials Science and Engineering of Nanyang Technological University as an assistant professor in early 2008 and became a full Professor in 2018. Yan's research efforts have been mainly devoted to two areas: (1) advanced electrode materials for energy storage devices; (2) high-efficiency thermoelectric semiconductor.